Predicting Precision Matrices for Color Matching

中本, 尊元

https://hdl.handle.net/2324/2236046

出版情報：Kyushu University, 2018, 博士（機能数理学）, 課程博士
バージョン：
権利関係：

Predicting Precision Matrices for Color Matching

Takayoshi Nakamoto

2019/1/27

Contents

Chapter 1

Introduction

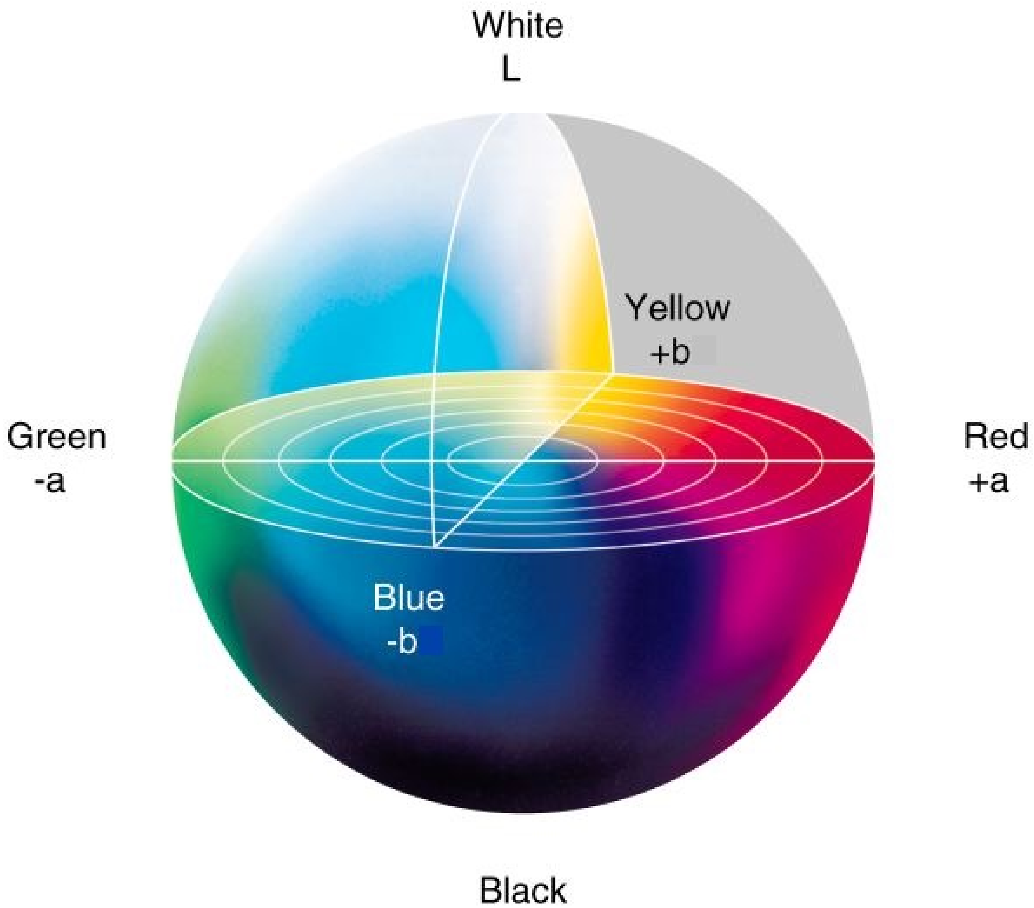

Figure 1.1: CIE Lab color coordinate system

At the development of the new color or texture in a car motor company, it is very important to match the color between products or parts in order to produce the good appearance and design. At first, we review color coordinate systems briefly.

The CIE Lab system (Commission Internationale de l'Eclairage) [1] is one of color coordinate systems. Each color in the system is represented by L (lightness), a for the green-red and b for the blue-yellow color components[3]. Figure 1.1 shows CIE-Lab system of colors. The lightness L takes the value from 0 to 100, whereas a and b are ranging from -90 to 90 degrees.

The human visual system has a dead zone characteristic, i.e., a set of colors with little difference is visually recognized as the same color[4]. This dead zone is represented by an ellipsoid in the Lab space with the color center of interest[6]. Then, prediction of a dead zone ellipsoid corresponding to a new color is required to know the acceptable zone in the Lab space (**the color matching problem**).

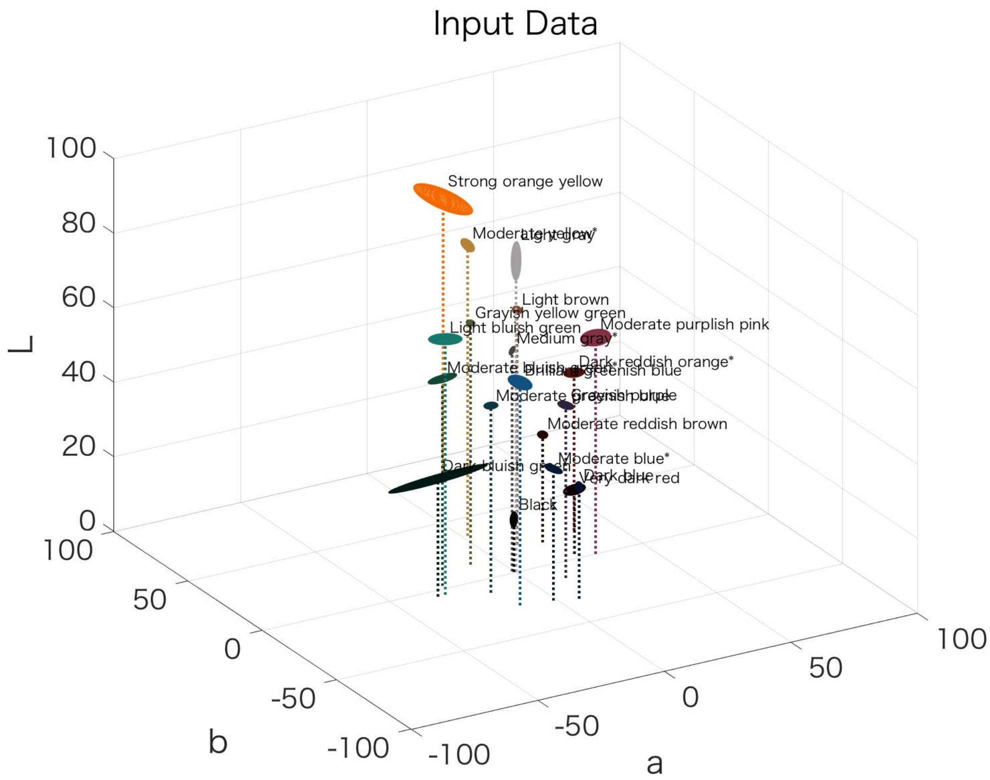

Figure 1.2: Ellipsoids for DuPont data set

The DuPont dataset[7] gives 19 pairs of colors and ellipsoids in the Lab space. See Figure 1.2 for color centers and corresponding ellipsoids. Note that shapes of ellipsoids are different color to color. It is also seen that similar colors have similar shapes in Lab space[8]. For examples, "Strong orange yellow" and "Moderate yellow" have similar shapes with long and thin for the b coordinate. Also, "Moderate green", "Moderate bluish green", and "Dark bluish green" have similar shapes with long and thin for a coordinate.

The dataset is represented as $(\boldsymbol{u}_i, \boldsymbol{G}_i)$ for $i = 1, 2, ..., 19$, where $\boldsymbol{u}_i = (a_i, b_i, L_i)^T$ denote color centers, and $\boldsymbol{G}_i = (g_{ijk})$, $j, k = 1, 2, 3$ denote precision matrices (positive definite matrices) giving ellipsoids for colors $\boldsymbol{u}_i$. The dataset will be given in Section 2.

The problem considered here is to predict an ellipsoid or a positive definite matrix for a new color center given as $\boldsymbol{u}_0 = (a_0, b_0, L_0)^T \in [-90, 90]^2 \times [0, 100]$. Then, the tolerance ellipsoid for the color with center $\boldsymbol{u}_0$ is given by an ellipsoid:

$$(\boldsymbol{v} - \boldsymbol{u}_0)^{\mathrm{T}} \mathbf{G}(\boldsymbol{u}_0) (\boldsymbol{v} - \boldsymbol{u}_0) \leq 1 \tag{1.1}$$

where $\boldsymbol{v} = (a, b, L)^T$ is a vector of variables in the Lab space, and

$$\mathbf{G}(\boldsymbol{u}_\mathbf{0}) = \begin{pmatrix} g_{11}(\boldsymbol{u}_\mathbf{0}) & g_{12}(\boldsymbol{u}_0) & g_{13}(\boldsymbol{u}_0) \\ g_{12}(\boldsymbol{u}_\mathbf{0}) & g_{22}(\boldsymbol{u}_0) & g_{23}(\boldsymbol{u}_0) \\ g_{13}(\boldsymbol{u}_\mathbf{0}) & g_{23}(\boldsymbol{u}_0) & g_{33}(\boldsymbol{u}_0) \end{pmatrix} \tag{1.2}$$

is a positive definite matrix corresponding to the color with center $\boldsymbol{u}_0$. In the sequel, we will estimate $\mathbf{G}(\boldsymbol{u}_0)$ through nonparametric and parametric methods in Sections 2 and 3 respectively.

We consider three metrics between positive definite matrices as the accuracy assessment of the estimated ellipsoids. We also consider three normalizing methods for Gaussian weights to the observed positive definite matrices. Then, we developed a nonparametric method of Nadaraya-Watson type estimation based on Gaussian kernel with several bandwidth parameters. Furthermore, we propose a matrix-valued regression to logarithm of positive definite matrices as response variables and three elements of color centers as explanatory variables.

The best result was obtained by the nonparametric methods with three bandwidth parameters. The log normal regression shows weaker performance. Its model estimation, however, is easily carried out. The both of the proposed methods would greatly reduce the cost of color matching compared with the conventional cut-and-try method. This would make the development of new colors more efficient.

Chapter 2

Nonparametric prediction of positive definite matrices

The ellipsoid (1.1) of the color $\boldsymbol{u}_i = (a_i, b_i, L_i)^T$ $(i = 1, 2, \ldots, 19)$ in the DuPont dataset is rewritten as follow.

$$(\boldsymbol{v} - \boldsymbol{u}_i)^{\mathrm{T}} \boldsymbol{V}_i^{-1} (\boldsymbol{v} - \boldsymbol{u}_i) \leq 1 \tag{2.1}$$

where $\boldsymbol{v} = (a, b, L)^T$ and

$$\boldsymbol{V}_i = \begin{pmatrix} v_{i11} & v_{i12} & v_{i13} \\ v_{i12} & v_{i22} & v_{i23} \\ v_{i13} & v_{i23} & v_{i33} \end{pmatrix} \tag{2.2}$$

is a positive definite matrix corresponding to the variance-covariance matrix. Table 2.1 lists color names, centers $\boldsymbol{u}_i$ and matrices $\boldsymbol{V}_i$ of the DuPont dataset.

Table 2.1: Color names, centers and ellipsoids from the DuPont dataset

Center Names	a	b	L	v_{11}	v_{22}	v_{12}	v_{13}	v_{23}	v_{33}
Moderate blue	-1.40	-27.81	35.34	1.78	5.02	-1.17	-0.05	0.27	0.85
Moderate greenish blue	-16.37	-11.26	50.26	2.56	2.34	0.12	-0.07	-0.03	0.62
Medium gray	-0.78	1.05	59.33	0.78	1.96	-0.13	0.03	0.13	0.78
Moderate bluish green	-27.55	2.37	55.62	5.89	1.75	-0.36	-0.30	0.15	0.95
Light brown	12.61	20.57	62.93	1.74	2.30	0.37	0.02	0.15	0.88
Grayish purple	12.15	-13.08	46.39	2.11	3.73	-0.96	0.03	-0.08	0.81
Dark reddish orange	35.65	21.40	42.32	3.66	2.80	0.59	-0.09	0.11	1.04
Moderate yellow	1.94	35.64	78.02	1.65	4.13	0.25	-0.02	0.21	1.29
Grayish yellow green	-10.01	13.28	64.94	1.43	2.36	-0.28	-0.14	0.14	0.76
Black	-0.45	0.42	14.14	0.63	2.10	-0.06	0.01	-0.06	1.52
Light bluish green	-30.73	-5.03	68.68	6.13	4.07	-1.13	-0.42	0.11	1.09
Moderate reddish brown	21.12	17.80	28.89	1.24	2.63	0.41	-0.09	-0.20	1.03
Dark bluish green	-33.64	-5.01	31.68	21.94	1.52	1.60	-1.52	0.02	1.27
Brilliant greenish blue	-13.44	-25.90	59.90	3.12	5.60	-1.25	-0.04	-0.54	1.30
Very dark red	25.24	3.41	17.36	4.26	2.69	-0.18	-0.26	0.26	1.25
Moderate purplish pink	31.51	-0.18	58.11	5.83	3.99	-0.42	0.08	-0.12	1.74
Dark blue	6.83	-31.15	30.19	1.77	3.03	-1.10	-0.01	-0.01	1.07
Light gray	0.31	0.21	83.48	1.10	5.28	-0.51	0.15	-0.10	1.90
Strong orange yellow	18.23	79.89	76.06	3.47	19.34	-0.03	0.19	0.66	2.40

2.1 Normalization of input vectors

Hereafter, color centers $\boldsymbol{u}_i = (a_i, b_i, L_i)^T$ are used for expression of $\boldsymbol{V}_i$. Table 2.2 summarizes basic statistics of Table 2.1. It is seen that sample means are largely different. Therefore, we consider the following normalization methods for deriving Gaussian kernel weights.

Table 2.2: Basic statistics of color centers

	Sample means	Standard deviations	Minimum	Maximum
a_i	1.641	20.236	-33.638	35.646
b_i	4.034	25.276	-31.146	79.894
L_i	50.717	20.289	14.140	83.481

First normalization method Let $\boldsymbol{u} = (a, b, L)^T \in [-90, 90]^2 \times [0, 100]$ denote a color in Lab space. Then, we define the following normalization:

$$\psi_1(\boldsymbol{u}) = \left(\frac{a}{90}, \frac{b}{90}, \frac{L}{50} - 1\right) \in [-1, 1]^3 \tag{2.3}$$

where we take denominators 90 or 50 so that the transformed values belong into an interval $[-1, 1]$.

Second normalization method The second normalization is based on sample means and standard deviations.

$$\psi_2\left(\boldsymbol{u}\right) = \left(\frac{a-\bar{a}}{s_a}, \frac{b-\bar{b}}{s_b}, \frac{L-\bar{L}}{s_L}\right) \in \mathbb{R}^3 \tag{2.4}$$

where $\bar{a}$ and s_a^2 denote the sample means and the sample variance of a_i. Similarly, $\bar{b}$, s_b^2, $\bar{L}$, and s_L^2 are defined.

Third normalization method The third normalization is to transform $\boldsymbol{u}$ into the unit cube as

$$\psi_3\left(\boldsymbol{u}\right) = \left(\frac{a-a_{\min}}{a_{\max}-a_{\min}}, \frac{b-b_{\min}}{b_{\max}-b_{\min}}, \frac{L-L_{\min}}{L_{\max}-L_{\min}}\right) \in \left[0,1\right]^3 \tag{2.5}$$

where $a_{\min} = \min\left\{a_1, \cdots, a_n\right\}$. Similarly, $a_{\max}$, $b_{\min}$, $b_{\max}$, $L_{\min}$ and $L_{\max}$ are defined.

2.2 Metrics between positive definite matrices

Let $\mathbf{L} = \left(\, l_{jk} \,\right)$ and $\mathbf{M} = \left(\, m_{jk} \,\right)$ be positive definite matrices of order 3. We use the following three metrics for evaluating the positive definite matrices in order to obtain the best Gaussian kernel estimations.

Frobenius norm The Frobenius norm gives the Euclidean norm between two matrices.

$$\Delta_F\left(\mathbf{L},\mathbf{M}\right) = \left\|\mathbf{L}-\mathbf{M}\right\|_F = \sqrt{\sum_{j=1}^{3}\sum_{k=1}^{3}\left(l_{jk}-m_{jk}\right)^2} \tag{2.6}$$

Riemannian metric The Riemannian metric is obtained from the geometrical distance between two matrices[12].

$$\Delta_R(\mathbf{L},\mathbf{M}) = \sqrt{\sum_{j=1}^{3}\left\{\log\lambda_j\left(\mathbf{L}^{-1}\mathbf{M}\right)\right\}^2} \tag{2.7}$$

where $\lambda_j\left(\mathbf{L}^{-1}\mathbf{M}\right) > 0$ denotes the j-th largest eigenvalue of $\mathbf{L}^{-1}\mathbf{M}$.

Kullback Leibler (KL) divergence We apply the KL divergence between $N(\mathbf{0}, \mathbf{L})$ and $N(\mathbf{0}, \mathbf{M})$ by regarding two matrices as the variance-covariance matrices of two independent Gaussian distributions having zero mean.

$$\Delta_{KL}(\mathbf{L}, \mathbf{M}) = \frac{1}{2}\left\{\log\left|\mathbf{L}^{-1}\mathbf{M}\right| + \mathrm{trace}\left(\mathbf{L}^{-1}\mathbf{M}\right) - 3\right\} \tag{2.8}$$

The first two metrics satisfy the three axioms of the distance whereas KL does not.

2.3 Nonparametric estimation of a center matrix by Gaussian kernel

Gaussian kernel estimation is applied to the positive definite matrices [19]. We set $\mathcal{V}$ as the space containing all positive definite matrices of order p. Assume that training data set $\{\boldsymbol{V}_i \in \mathcal{V} \mid i = 1, \cdots, n\}$ is available. Then, our aim here is to derive an ellipsoid i.e. **a matrix** $\boldsymbol{V} \in \mathcal{V}$ of the training data **in some sense**. The matrix is defined by minimizing the following loss function:

$$L(\boldsymbol{V}) = \sum_{i=1}^{n} w_i \Delta_{KL}(\boldsymbol{V}, \boldsymbol{V}_i) \quad \text{for weights } w_i > 0 \text{ with } \sum_i w_i = 1 \tag{2.9}$$

where $\Delta_{KL}(\cdot, \cdot)$ is the KL divergence defined by (2.8).

Proposition Let

$$\hat{\boldsymbol{V}} = \sum_{i=1}^{n} w_i \boldsymbol{V}_i \in \mathcal{V} \tag{2.10}$$

be a weighted sum of the training data. Then, it holds that

$$\hat{\boldsymbol{V}} = \arg\min_{\boldsymbol{V} \in \mathcal{V}} L(\boldsymbol{V}) \tag{2.11}$$

Proof We obtain that

$$2L(\hat{\boldsymbol{V}}) = \sum_i w_i \left[\mathrm{trace}\left(\boldsymbol{V}_i\hat{\boldsymbol{V}}^{-1}\right) - p + \log\left|\boldsymbol{V}_i\hat{\boldsymbol{V}}^{-1}\right|\right]$$

By the linearity of the trace function, we have

$$\begin{aligned} 2L(\boldsymbol{V}) - 2L(\hat{\boldsymbol{V}}) &= \mathrm{trace}\left(\boldsymbol{V}^{-1}\hat{\boldsymbol{V}}\right) - \log|\boldsymbol{V}| - p + \log\left|\hat{\boldsymbol{V}}\right| \\ &= \mathrm{trace}\left(\boldsymbol{V}^{-1}\hat{\boldsymbol{V}}\right) - p + \log\left|\boldsymbol{V}^{-1}\hat{\boldsymbol{V}}\right| \geq 0 \end{aligned}$$

The last inequality follows from the non-negativity for KL divergence (2.8). Note that the equality holds if and only if $\boldsymbol{V} = \hat{\boldsymbol{V}}$.

Proposition implies that the weighted sum (2.10) minimizes the loss function (2.9). In the sequel, determination methods of the weights w_i are proposed from different viewpoints.

2.3.1 Gaussian kernel estimation 1

In the first method for predicting the positive definite matrix for a certain color center $\boldsymbol{u}$, we normalize input vector $\boldsymbol{u}$ and obtain $\psi_q(\boldsymbol{u})$ defined by (2.3) to (2.5) for $q = 1, 2, 3$. Next, we apply a single bandwidth tuning parameter $\gamma > 0$ to the nonlinear weighting function:

$$\hat{\boldsymbol{V}}(\psi_q(\boldsymbol{u})) = \sum_{i=1}^{n} w_i(\psi_q(\boldsymbol{u}), \gamma)\boldsymbol{V}_i \tag{2.12}$$

$$\text{where } w_i(\psi_q(\boldsymbol{u}), \gamma) = \frac{\exp\left\{-\gamma\left\|\psi_q(\boldsymbol{u}) - \psi_q(\boldsymbol{u}_i)\right\|^2\right\}}{\sum_{l=1}^{n}\exp\left\{-\gamma\left\|\psi_q(\boldsymbol{u}) - \psi_q(\boldsymbol{u}_l)\right\|^2\right\}}. \tag{2.13}$$

If $\gamma = 0$, (2.12) gives the mean matrix of $\boldsymbol{V}_i$. The positive definiteness of the matrix given by (2.12) is easily shown because it is given by the sum of positive weights on positive definite matrices.

The validity of estimation using the weighted sum in the form of (2.13) is ensured by Proposition. The bandwidth parameter $\gamma > 0$ is tuned by minimizing a metric between the estimated and observed positive definite matrices using leave-one-out cross-validation. We consider three types of metrics: the Frobenius norm, the Riemannian metric, and the KL divergence.

Let $\hat{\boldsymbol{V}}_i$ be the estimated positive definite matrix in the form of (2.12) with (2.13) using the training data with omitting $\boldsymbol{V}_i$. We tune parameter γ using the three metrics.

Frobenius norm

$$\hat{\gamma}_F = \arg\min_{\gamma>0} \sum_{i=1}^{n} \Delta_F^2 \left(\boldsymbol{V}_i, \hat{\boldsymbol{V}}_i\right) \tag{2.14}$$

where $\Delta_F(\cdot,\cdot)$ denotes the Frobenius norm (2.6).

Riemannian metric

$$\hat{\gamma}_R = \arg\min_{\gamma>0} \sum_{i=1}^{n} \Delta_R^2 \left(\boldsymbol{V}_i, \hat{\boldsymbol{V}}_i\right) \tag{2.15}$$

where $\Delta_R(\cdot,\cdot)$ denotes the Riemannian metric (2.7).

KL divergence

$$\hat{\gamma}_{KL} = \arg\min_{\gamma>0} \sum_{i=1}^{n} \Delta_{KL} \left(\boldsymbol{V}_i, \hat{\boldsymbol{V}}_i\right) \tag{2.16}$$

where $\Delta_{KL}(\cdot,\cdot)$ denotes the KL divergence (2.8).

2.3.2 Gaussian kernel estimation 2

The diagonal elements in positive definite matrix $\boldsymbol{V}$ are important than the off-diagonal elements because these parameters determine the ellipsoidal size corresponding to the color coordinates. We thus deconstruct the positive definite matrix $\boldsymbol{V}\left(\psi_q(\boldsymbol{u})\right)$ to the standard deviations and correlations as:

$$\boldsymbol{V}\left(\psi_q(\boldsymbol{u})\right) = \boldsymbol{S}\left(\psi_q(\boldsymbol{u})\right) \boldsymbol{C}\left(\psi_q(\boldsymbol{u})\right) \boldsymbol{S}\left(\psi_q(\boldsymbol{u})\right) \tag{2.17}$$

where

$$\boldsymbol{S}\left(\psi_q(\boldsymbol{u})\right) = \begin{pmatrix} \sqrt{v_{11}\left(\psi_q(\boldsymbol{u})\right)} & 0 & 0 \\ 0 & \sqrt{v_{22}\left(\psi_q(\boldsymbol{u})\right)} & 0 \\ 0 & 0 & \sqrt{v_{33}\left(\psi_q(\boldsymbol{u})\right)} \end{pmatrix} \tag{2.18}$$

$$\boldsymbol{C}\left(\psi_q(\boldsymbol{u})\right) = \begin{pmatrix} 1 & \rho_{12}\left(\psi_q(\boldsymbol{u})\right) & \rho_{13}\left(\psi_q(\boldsymbol{u})\right) \\ \rho_{12}\left(\psi_q(\boldsymbol{u})\right) & 1 & \rho_{23}\left(\psi_q(\boldsymbol{u})\right) \\ \rho_{13}\left(\psi_q(\boldsymbol{u})\right) & \rho_{23}\left(\psi_q(\boldsymbol{u})\right) & 1 \end{pmatrix} \tag{2.19}$$

The standard deviations and correlations are estimated using different bandwidths $\gamma > 0$ and $\delta > 0$ as

$$\sqrt{v_{jj}\left(\psi_q(\boldsymbol{u})\right)} = \sum_{i=1}^{n} w_i\left(\psi_q(\boldsymbol{u}), \gamma\right)\sqrt{v_{ijj}},\ j = 1, 2, 3 \tag{2.20}$$

$$\rho_{jk}\left(\psi_q(\boldsymbol{u})\right) = \sum_{i=1}^{n} w_i\left(\psi_q(\boldsymbol{u}), \delta\right)\rho_{ijk} \tag{2.21}$$

$$,\ (j,k) = (1,2), (1,3), (2,3)$$

$$w_i\left(\psi_q(\boldsymbol{u}), \gamma\right) = \frac{\exp\left\{-\gamma\left\|\psi_q(\boldsymbol{u}) - \psi_q(\boldsymbol{u}_i)\right\|^2\right\}}{\sum_{l=1}^{n}\exp\left\{-\gamma\left\|\psi_q(\boldsymbol{u}) - \psi_q(\boldsymbol{u}_l)\right\|^2\right\}} \tag{2.22}$$

The ρ_{ijk} is the (j,k) correlation of matrix $\boldsymbol{V}_i$. Two bandwidths are estimated by minimizing the metric as

Frobenius norm

$$\left(\hat{\gamma}_F, \hat{\delta}_F\right) = \arg\min_{\gamma>0,\ \delta>0}\sum_{i=1}^{n}\Delta_F^2\left(\boldsymbol{V}_i, \hat{\boldsymbol{V}}_i\right) \tag{2.23}$$

where $\hat{\boldsymbol{V}}_i$ is derived using (2.17) with two parameters , and $\Delta_F(\cdot,\cdot)$ denotes the Frobenius norm (2.6).

Riemannian metric

$$\left(\hat{\gamma}_R, \hat{\delta}_R\right) = \arg\min_{\gamma>0, \delta>0}\sum_{i=1}^{n}\Delta_R^2\left(\boldsymbol{V}_i, \hat{\boldsymbol{V}}_i\right) \tag{2.24}$$

where $\Delta_R(\cdot,\cdot)$ denotes the Riemannian metric (2.7).

KL divergence

$$\left(\hat{\gamma}_{KL}, \hat{\delta}_{KL}\right) = \arg\min_{\gamma>0,\delta>0} \sum_{i=1}^{n} \Delta_{KL}\left(\boldsymbol{V}_i, \hat{\boldsymbol{V}}_i\right) \tag{2.25}$$

where $\Delta_{KL}(\cdot,\cdot)$ denotes the KL divergence (2.8).

Note that the tuned parameters depend on the normalization methods $\psi_q(\cdot)$. Note also that $\hat{\boldsymbol{V}}_i$ is positive definite because its correlation matrix is given by a linear combination of training correlation matrices with positive weights.

2.3.3 Gaussian kernel estimation 3

First and second estimation methods in 2.3.1 and 2.3.2 use the common parameter γ for the variances v_{11}, v_{22}, and v_{33} for normalization types $q = 1, 2, 3$. Actually, the maximum and the minimum of v_{i11} is given by 1.600 and 0.054 respectively (see Table 2.1). This means v_{11} corresponding to color coordinate a and other two variances should be modeled separately. Under this consideration, we will propose the following third model.

$$\begin{aligned}
\sqrt{v_{11}\left(\psi_q(\boldsymbol{u})\right)} &= \sum_{i=1}^{n} w_i\left(\psi_q(\boldsymbol{u}), \gamma\right)\sqrt{v_{i11}}, && (2.26)\\
\sqrt{v_{jj}\left(\psi_q(\boldsymbol{u})\right)} &= \sum_{i=1}^{n} w_i\left(\psi_q(\boldsymbol{u}), \delta\right)\sqrt{v_{ijj}}, \quad j = 2, 3 && (2.27)\\
\rho_{jk}\left(\psi_q(\boldsymbol{u})\right) &= \sum_{i=1}^{n} w_i\left(\psi_q(\boldsymbol{u}), \eta\right)\rho_{ijk} && (2.28)\\
& \quad , \ (j,k) = (1,2), (1,3), (2,3)
\end{aligned}$$

Then, three bandwidths are tuned as follows.

Frobenius norm

$$\left(\hat{\gamma}_F, \hat{\delta}_F, \hat{\eta}_F\right) = \arg\min_{\gamma>0,\ \delta>0,\ \eta>0} \sum_{i=1}^{n} \Delta_F^2\left(\boldsymbol{V}_i, \hat{\boldsymbol{V}}_i\right) \tag{2.29}$$

where $\hat{\boldsymbol{V}}_i$ is estimated using (2.17) with three bandwidths , and $\Delta_F(\cdot,\cdot)$ is the Frobenius norm (2.6).

Riemannian metric

$$\left(\hat{\gamma}_R, \hat{\delta}_R, \hat{\eta}_R\right) = \arg \min_{\gamma>0,\delta>0,\eta>0} \sum_{i=1}^{n} \Delta_R^2 \left(\boldsymbol{V}_i, \hat{\boldsymbol{V}}_i\right) \tag{2.30}$$

where $\Delta_R(\cdot,\cdot)$ is the Riemannian metric (2.7).

KL divergence

$$\left(\hat{\gamma}_{KL}, \hat{\delta}_{KL}, \hat{\eta}_{KL}\right) = \arg \min_{\gamma>0,\delta>0,\eta>0} \sum_{i=1}^{n} \Delta_{KL} \left(\boldsymbol{V}_i, \hat{\boldsymbol{V}}_i\right) \tag{2.31}$$

where $\Delta_{KL}(\cdot,\cdot)$ is the KL divergence (2.8).

Note that $\hat{\boldsymbol{V}}_i$ is positive definite by the same reason stated in two-bandwidth case.

2.4 Numerical experiments through DuPont dataset

The proposed nonparametric formulas up to three bandwidths based on three normalization methods were applied to the DuPont training dataset. We have 9 ($= 3^2$) possible prediction formulas for positive definite matrices. The bandwidths were tuned by the leave-one-out cross validation according to the three metrics between observed and predicted matrices.

Table 2.3 compares 27 ($= 3^3$) models and lists tuned bandwidths. The first row separated the models according to the number of widths one, two and three corresponding to formulas (2.14), (2.23) and (2.29). The second row implies the qth normalization methods with $q = 1, 2, 3$ for each block. The 2nd entry of the 4th row, 727.9, gives the minimum Frobenius norm appeared in (2.14) with the optimal bandwidth based on the first normalization method $q = 1$. The 9th entry in the 4th row, 586.8 in bold face, gives the minimum Frobenius norm (2.29) in the same row. Similarly, numerals in bold face at 5th and 6th rows mean that they are minimum in the respective rows. It is observed that Riemannian metric and KL divergence chosen the model with three bandwidths based on the third normalization method. The estimated bandwidths are tabulated from the 8th to 16th rows.

It is seen from Table 2.3 that the models with three bandwidths show the best performance. Furthermore, the second and third normalization methods works well, and the difference between the second and the third normalizations is small.

Table 2.3: Comparison of kernel estimation results

Number of bandwidths	One (2.12)			Two (2.20 to 2.21)			Three (2.26 to 2.28)		
Normalization methods: q	1 (2.3)	2 (2.4)	3 (2.5)	1 (2.3)	2 (2.4)	3 (2.5)	1 (2.3)	2 (2.4)	3 (2.5)
Metrics									
Frobenius norm	727.9	611.7	624.6	734.8	607.4	605.5	719.9	**586.8**	598.0
Riemannian metric	26.52	20.99	19.95	26.42	20.64	19.78	24.79	20.12	**19.54**
KL divergence	8.686	6.472	6.297	8.666	6.620	6.378	8.057	6.335	**6.286**
Bandwidths									
γ_F	21.89	132.1	132.1	20.31	183.4	832.1	0.031	200,1	1532
γ_R	25.59	1.771	29.80	13.47	1.563	28.63	0.031	2.250	36.78
γ_{KL}	1.217	1.506	26.18	0.031	1.656	33.47	0.031	200.0	44.59
δ_F	–	–	–	26.91	1.750	20.75	16.78	1.250	256.08
δ_R	–	–	–	18.06	1.313	17.44	11.84	0.844	15.81
δ_{KL}	–	–	–	93.25	1.250	15.72	13.19	0.938	18.50
η_F	–	–	–	–	–	–	16.47	1.813	21.00
η_R	–	–	–	–	–	–	20.19	1.281	17.13
η_{KL}	–	–	–	–	–	–	83.50	1.156	15.53

Results of calculation and minimization are shown from Figure 2.1 to 2.3 , in the case of the models with three parameters, and the second and third normalization method. Furthermore, the true ellipsoids are represented by Figure 2.4. Other combinations with the models having bandwidths and the normalization methods are displayed in Appendix A.

2.4.1 Estimated ellipsoids by the proposed methods

Figure 2.4 depicts the true (a) and estimated ellipsoids by the kernel methods (b)-(d). It is seen that all the models failed to estimate the flat-shaped ellipsoid of "Dark bluish green". This may come from the fact that this color is located in the edge of 19 training colors.

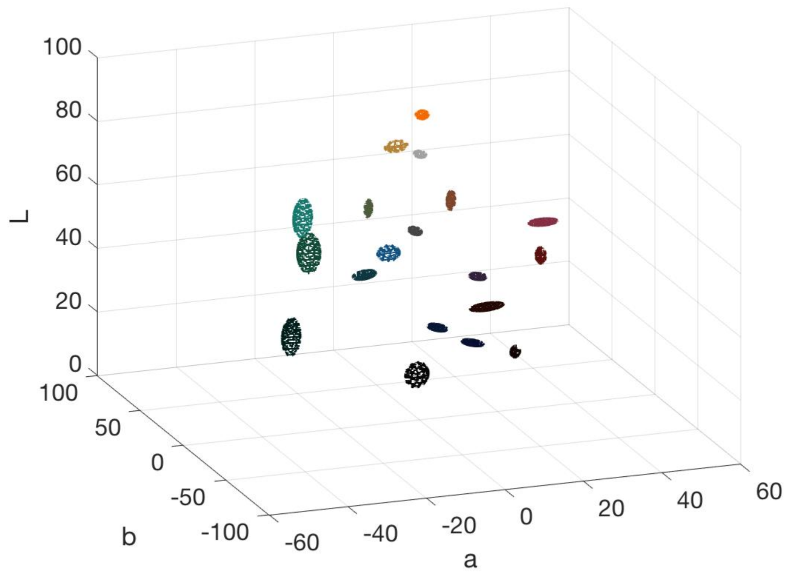

Figure 2.1: Frobenius norm and 2nd normalization

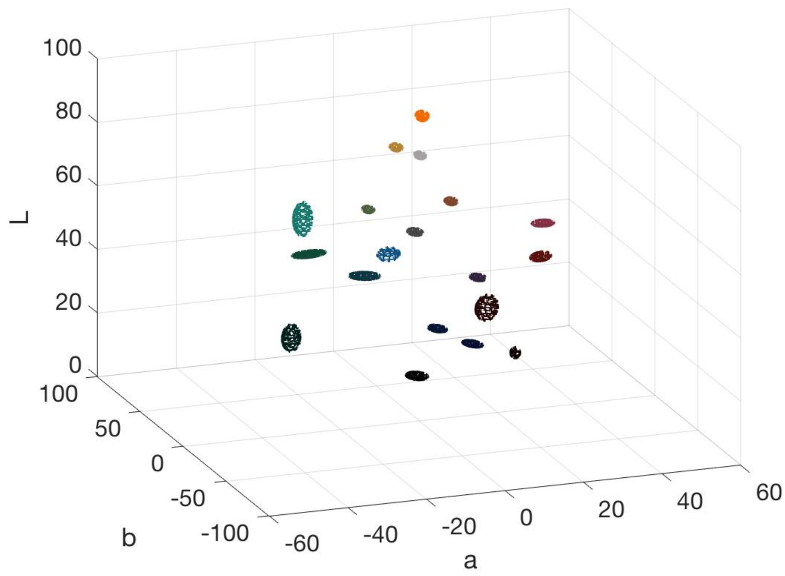

Figure 2.2: Riemannian metric and 3rd normalization

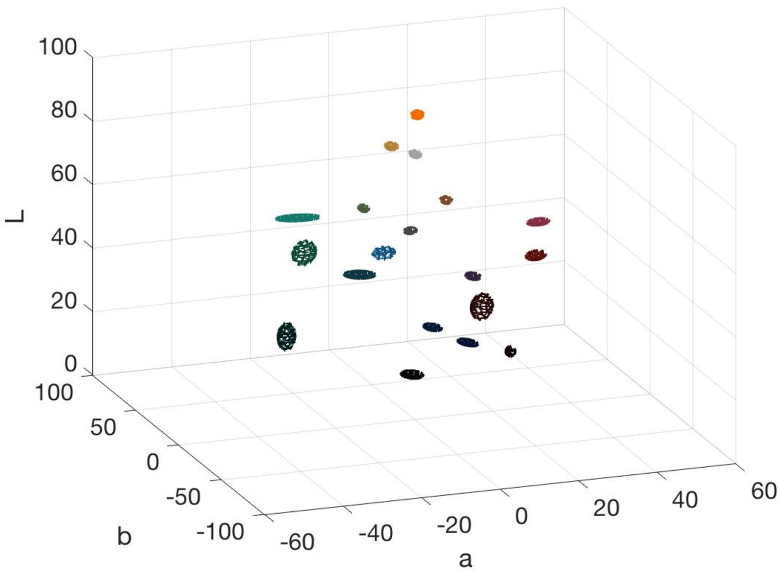

Figure 2.3: KL divergence and 3rd normalization

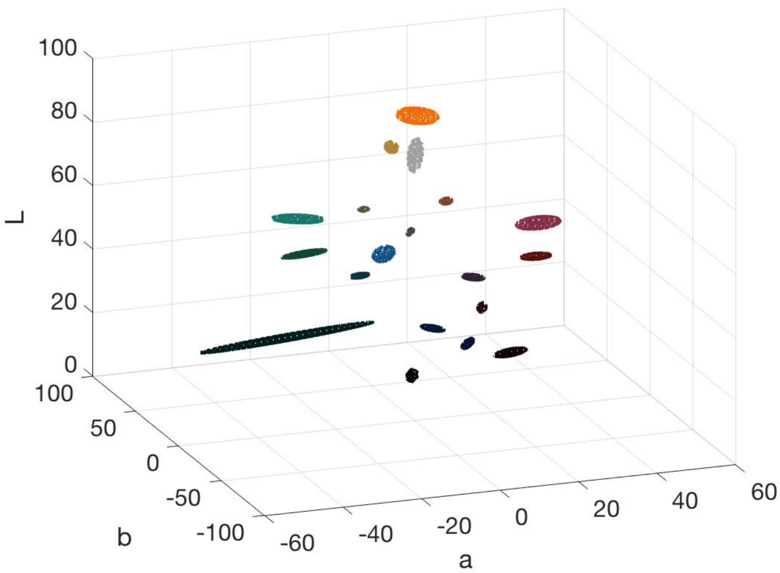

Figure 2.4: True ellipsoids of 19 colors

Chapter 3

Clustering of positive definite matrices

In previous chapter, it's seen that results of the Gaussian kernel estimation with three types of bandwidth parameters and normalization methods are different from the true positive definite matrices in the numerical experiment. It seems that the estimation using only positive definite matrices may be insufficiency. Then, it would like to re-examine the relationship between positive definite matrices and color values given as $\boldsymbol{u} = (a, b, L)^T$ in Chapter 1 by some statistical classification approaches.

3.1 Geometric mean of positive definite matrices as inverse of positive definite matrices

Let $\boldsymbol{V}_k$ and $\boldsymbol{V}_l$ are positive definite matrices with order of $p(=3)$, respectively. , where $k,\ l = 1, \cdots, n$. It's simply represented as $\boldsymbol{V}_k, \boldsymbol{V}_l > 0$. Then, the squared Riemannian metric (2.7) will be rewritten by

$$\Delta_R(\boldsymbol{V}_k, \boldsymbol{V}_l) = \sqrt{\sum_{j=1}^{p} \left\{ \log \lambda_j \left((\boldsymbol{V}_k)^{-1} \boldsymbol{V}_l \right) \right\}^2}, \tag{3.1}$$

where $\lambda_j \left((\boldsymbol{V}_k)^{-1} \boldsymbol{V}_l \right) > 0$ denotes the j-th eigenvalue of $(\boldsymbol{V}_k)^{-1} \boldsymbol{V}_l$. The geometric path from $\boldsymbol{V}_k$ to $\boldsymbol{V}_l$ is shown as follow

$$\boldsymbol{V}_k \#_t \boldsymbol{V}_l = (\boldsymbol{V}_k)^{1/2} \left((\boldsymbol{V}_k)^{-1/2} (\boldsymbol{V}_l) (\boldsymbol{V}_k)^{-1/2} \right)^t (\boldsymbol{V}_k)^{1/2} \quad \text{for } 0 \leq t \leq 1. \tag{3.2}$$

Let $\boldsymbol{V} = \{\boldsymbol{V}_m = \left(V_{m\alpha\beta} \right)_{\alpha,\beta=1,2,...,p} \mid i = 1,2,...,n\}$ be a training data set of positive definite matrices of order 3 , where V_m are positive definite matrices given as inverse of positive definites. We purpose a clustering method of the training data set. The geometric mean $\bar{\boldsymbol{V}}$ of $\boldsymbol{V}_1, \cdots, \boldsymbol{V}_n$ is defined by

$$\bar{\boldsymbol{V}} = \text{argmin}_{V>0} L(\boldsymbol{V}), \text{ where } L(\boldsymbol{V}) \equiv \sum_{l=1}^{n} \Delta_R(\boldsymbol{V}, \boldsymbol{V}_l)^2. \tag{3.3}$$

The following theorem is due to [15].

Theorem 3.1.1 *The geometric mean $\bar{\boldsymbol{V}}$ of $\boldsymbol{V}_1, \cdots, \boldsymbol{V}_n$ is given by*

$$\bar{\boldsymbol{V}} = \exp \left[\frac{1}{n} \{ \log(\boldsymbol{V}_1) + \log(\boldsymbol{V}_2) + \cdots + \log(\boldsymbol{V}_n)) \} \right] \tag{3.4}$$

when

$$\log \boldsymbol{V} = \mathbf{U} \begin{pmatrix} \log \lambda_1 & 0 & 0 \\ 0 & \log \lambda_2 & 0 \\ 0 & 0 & \log \lambda_3 \end{pmatrix} \mathbf{U}^T \tag{3.5}$$

Here

$$\boldsymbol{V} = \mathbf{U} \begin{pmatrix} \lambda_1 & 0 & 0 \\ 0 & \lambda_2 & 0 \\ 0 & 0 & \lambda_3 \end{pmatrix} \mathbf{U}^T \tag{3.6}$$

where $\lambda_1 > 0, \cdots > 0, \lambda_3 > 0$ are eigenvlaues of $\boldsymbol{V} > 0$ and $\mathbf{U}$ is an orthogonal matrix.

3.2 K - means for positive definite matrices

Using this theorem, we can propose the following for positive definite matrices give as inverse matrices of positive definites[16, 13].

1^{st} **step** . Set $t = 0$, and choose initial cluster centers by different matrices $\mathbf{C}_1^{(0)}, \cdots, \mathbf{C}_k^{(0)}$ selected randomly from $\boldsymbol{V}_1, \cdots, \boldsymbol{V}_n$.

t^{th} **step** .

- Allocate $\boldsymbol{V}_i$ into one of centers $\mathbf{C}_j^{(t)}$ which minimizes the squared distance by Frobenius norm or Riemannian metric shown in (2.6) and (2.7).

$$\Delta_F \left(\boldsymbol{V}_i,\ \mathbf{C}_j^{(t)} \right)^2 \tag{3.7}$$

$$\Delta_R \left(\boldsymbol{V}_i,\ \mathbf{C}_j^{(t)} \right)^2,\ j = 1, \cdots, k \tag{3.8}$$

- Construct k clusters $\mathcal{C}_j^{(t)}$ whose centers are given by $\mathbf{C}_j^{(t)},\ j = 1, \cdots, k$.
- Update cluster centers by geometric means

$$\mathbf{C}_j^{(t+1)} = \exp \left[\frac{\sum_{\boldsymbol{V}_i \in \mathcal{C}_j^{(t)}} \log(\boldsymbol{V}_i)}{\sum_{\boldsymbol{V}_i \in \mathcal{C}_j^{(t)}} 1} \right],\ j = 1, \cdots, k \tag{3.9}$$

- Set $t = t + 1$.

Repeat t^{th} steps until convergence. We apply the Frobenius norm and Riemannian metric to squared distance, respectively. Figure 3.1 (a) is result of clustering with three classes by K-means method and distance of Frobenius norm. Figure 3.1 (b) is also result of clustering with three classes by K-means method and distance of Riemannian metric.

Figure 3.2 (a) is result of clustering with four classes by K-means method and distance of Frobenius norm. Figure 3.2 (b) is result of clustering with four classes by K-means method and distance of Riemannian metric.

Figure 3.3 (a) is result of clustering with five classes by K-means method and distance of Frobenius norm. Figure 3.3 (b) is result of clustering with five classes by K-means method and distance of Riemannian metric.

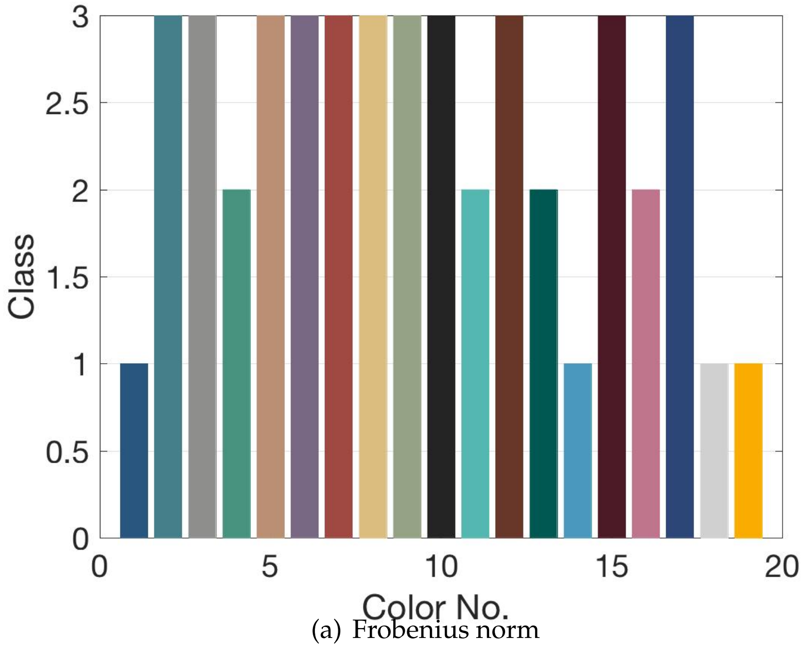

(a) Frobenius norm

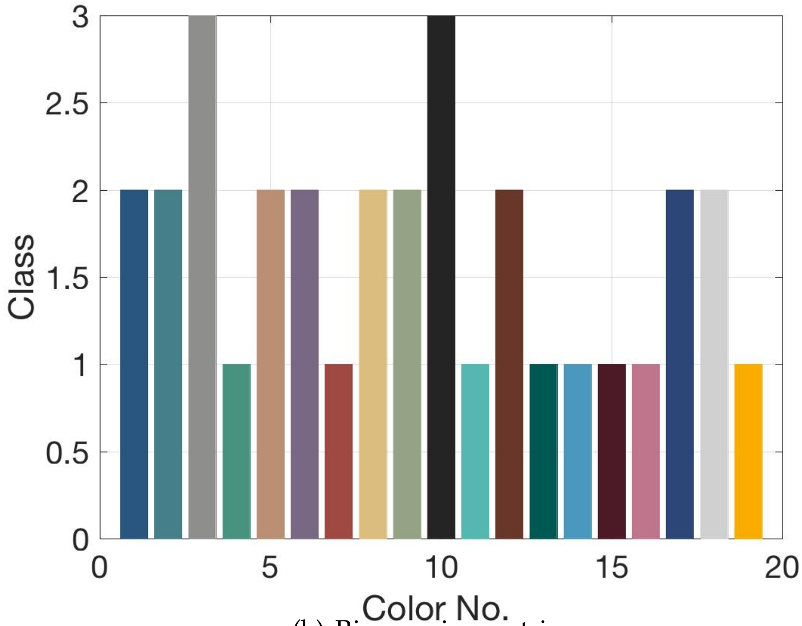

(b) Riemannian metric

Figure 3.1: Comparison of K - means results in the case of three classes

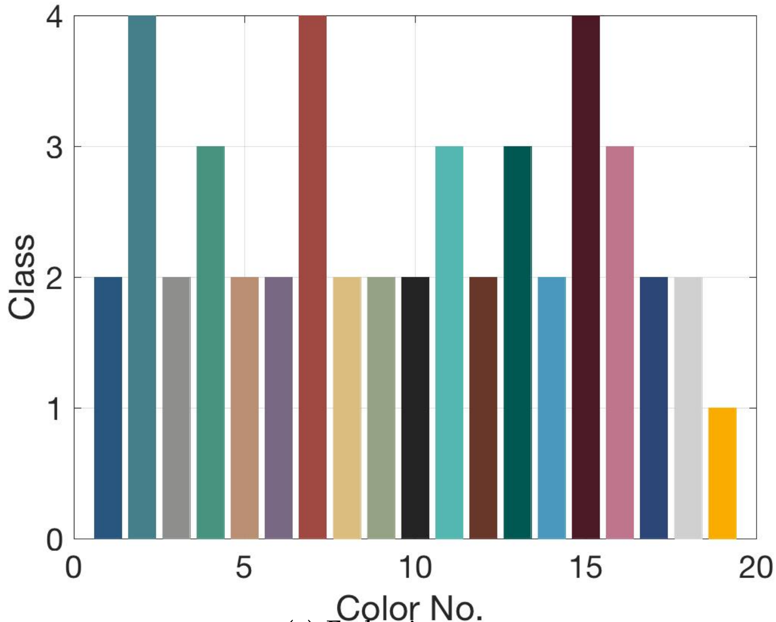

(a) Frobenius norm

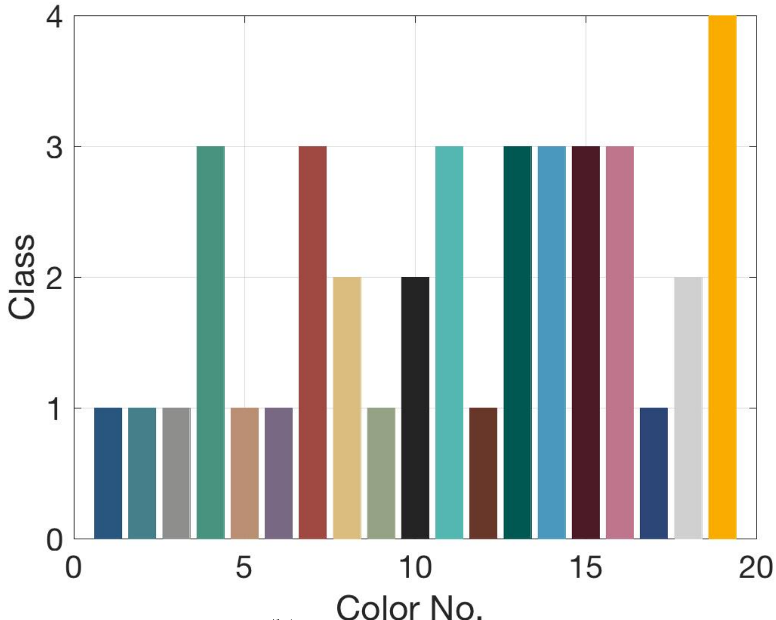

(b) Riemannian metric

Figure 3.2: Comparison of K - means results in the case of four classes

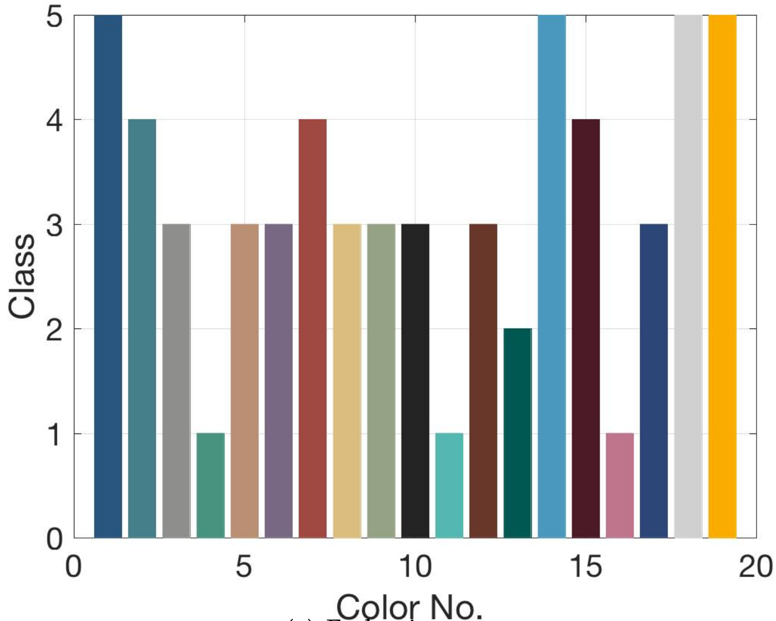

(a) Frobenius norm

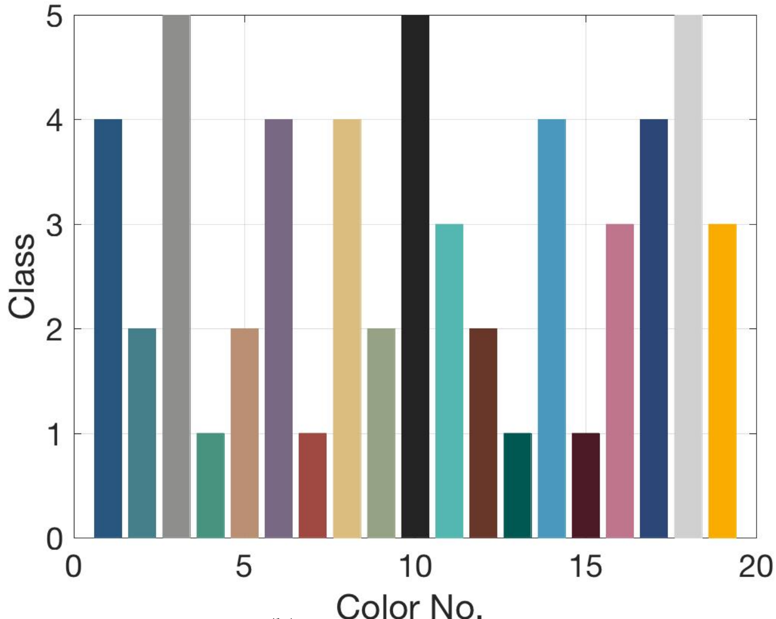

(b) Riemannian metric

Figure 3.3: Comparison of K - means results in the case of five classes

Therefore, classification results using only positive definite matrices could not find the relationship between positive definite matrices and color centers.

3.3 Ward's method for positive definite matrices

In addition, we will try to apply the hierarchical clustering to positive definite matrices in order to grasp the trend of them with ellipsoidal shape represented in Figure 1.2 and Table 2.1. For details, we will use the linkage clustering with the Ward's method[17]. In this method, the distance $d(C_p,\ C_q)$ between class C_p and class $C_q,\ p,\ q = 1,\ \cdots,\ n$ is defined as follows,

$$d(C_p,\ C_q) = E(C_p \cup C_q) - E(C_p) - E(C_q) \tag{3.10}$$

where $E(C_p),\ p = 1,\ \cdots,\ n$ is the squared sum of distance from

$$E(C_p) = \sum_{\boldsymbol{V} \in C_p} \left(d(\boldsymbol{V},\ C_p)\right) \tag{3.11}$$

We apply the KL divergence for the distance $d(\boldsymbol{V},\ C_p),\ p = 1,\ \cdots,\ n$ as follow.

KL divergence

$$\Delta_{KL}\left(\boldsymbol{V}, C_p\right)^2 = \log \frac{|C_p|}{|\boldsymbol{V}|} + \mathrm{tr}\left(\boldsymbol{V}^{-1} C_p\right) + \Delta \boldsymbol{u}^T C_p \Delta \boldsymbol{u} - p \tag{3.12}$$

$$\Delta \boldsymbol{u} = \left(u - u_p\right)^T$$

where $u \in \mathbb{R}^{3\times 1}$ is input vector corresponding to $\boldsymbol{V}$, and $u_p \in \mathbb{R}^{3\times 1}$ is one doing to C_p.

The hierarchical clustering results by the single method for the KL divergence with the simple , the logarithm, and the squared are shown in Figure 3.4 to 3.6, respectively.

The hierarchical clustering results by the complete method for the KL divergence with the simple , the logarithm, and the squared are shown in Figure 3.7 to 3.9, respectively.

The hierarchical clustering results by the complete method for the KL divergence with the simple , the logarithm, and the squared are shown in Figure 3.10 to 3.12, respectively.

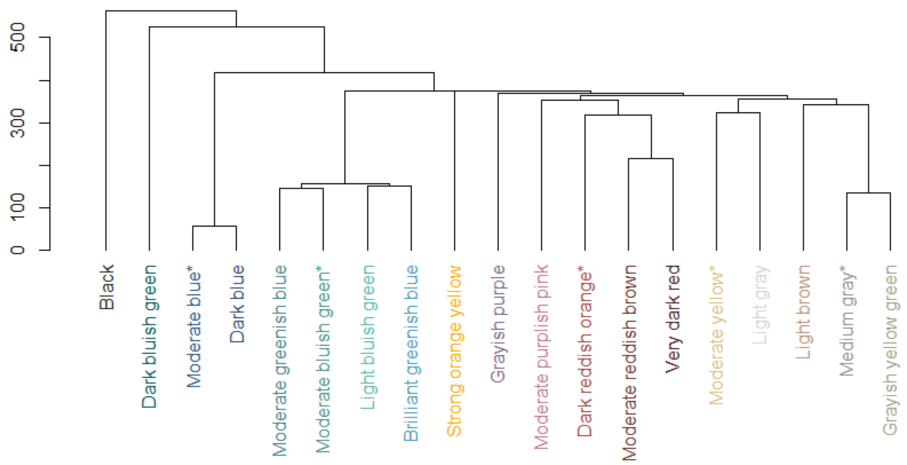

Figure 3.4: Dendrogram for the result of hierarchal clustering using the single method with distance of the KL divergence

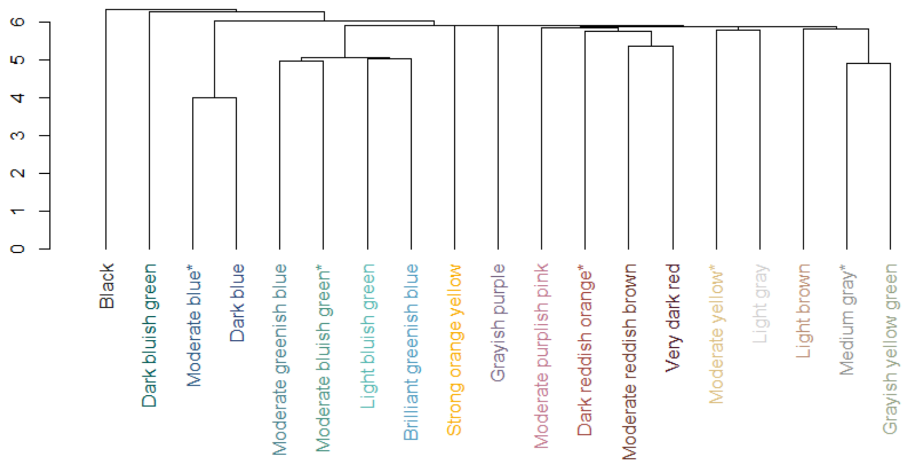

Figure 3.5: Dendrogram for result of hierarchal clustering using the single method with distance of the logarithm KL divergence

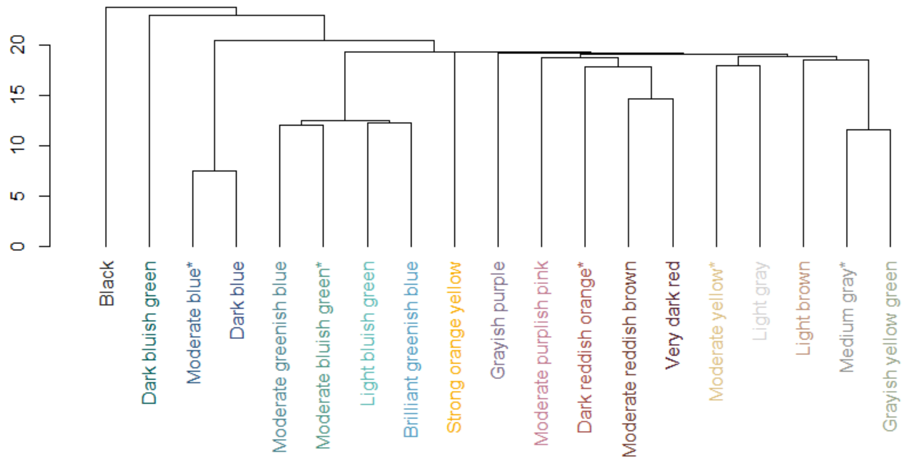

Figure 3.6: Dendrogram for result of hierarchal clustering using the single method with distance of the squared KL divergence

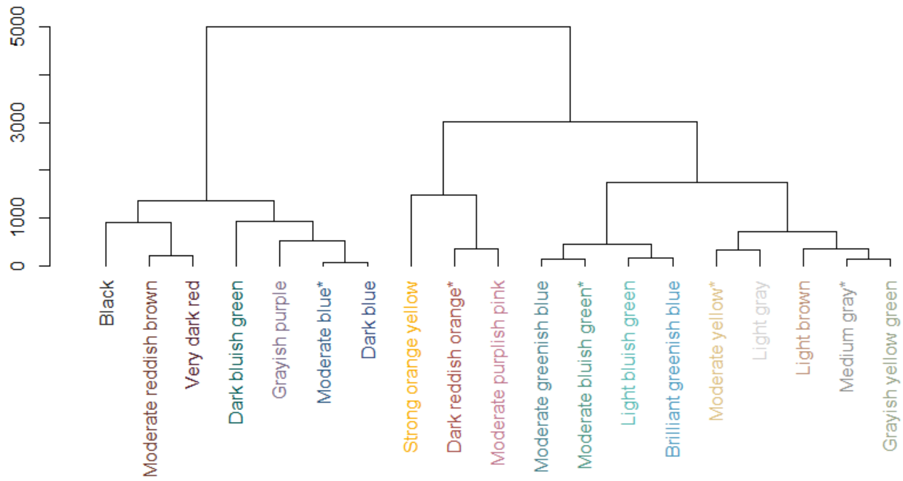

Figure 3.7: Dendrogram for the result of hierarchal clustering using the complete method with distance of the KL divergence

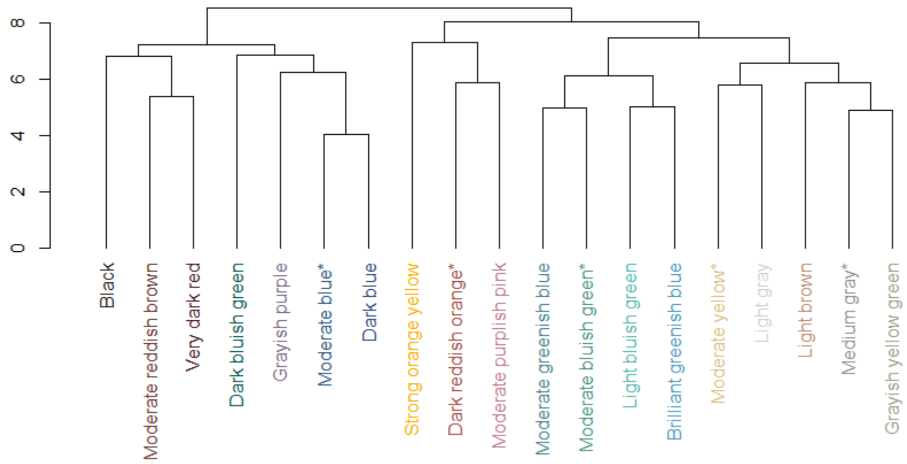

Figure 3.8: Dendrogram for result of hierarchal clustering using the complete method with distance of the logarithm KL divergence

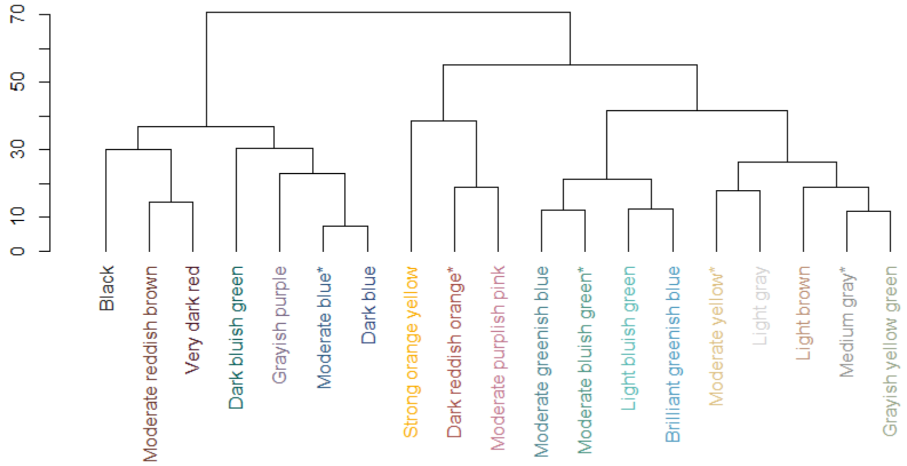

Figure 3.9: Dendrogram for result of hierarchal clustering using the complete method with distance of the squared KL divergence

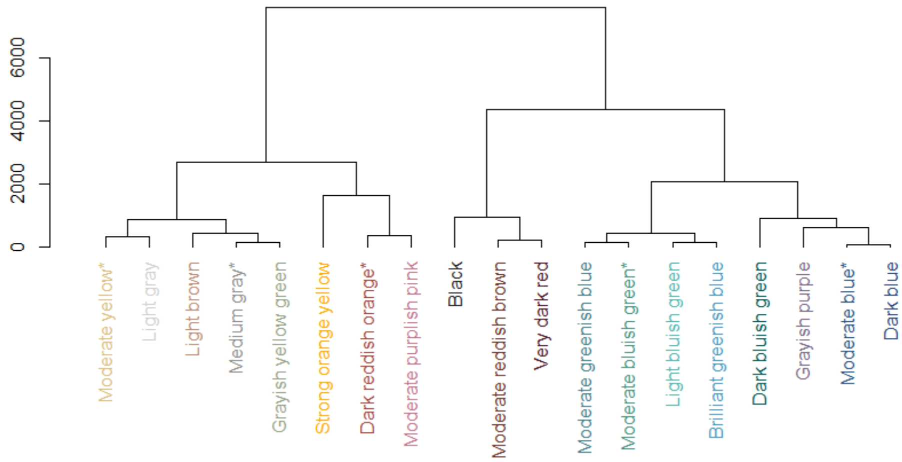

Figure 3.10: Dendrogram for the result of hierarchal clustering using the Ward method with distance of the KL divergence

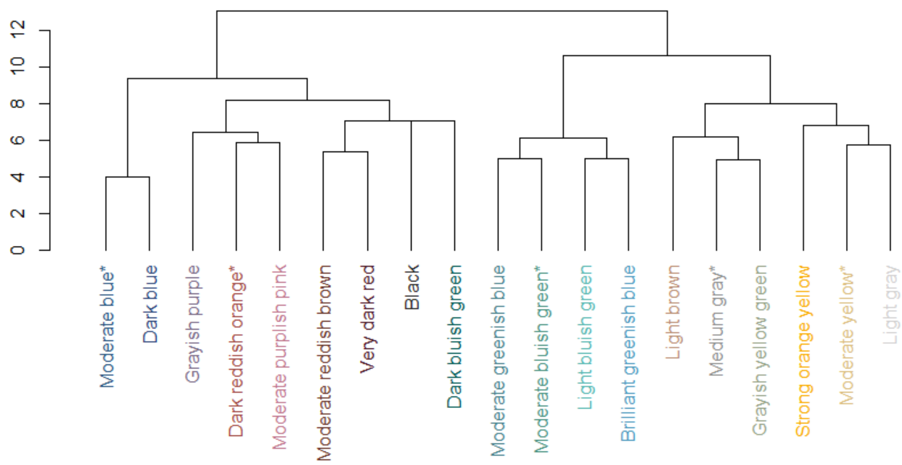

Figure 3.11: Dendrogram for result of hierarchal clustering using the Ward method with distance of the logarithm KL divergence

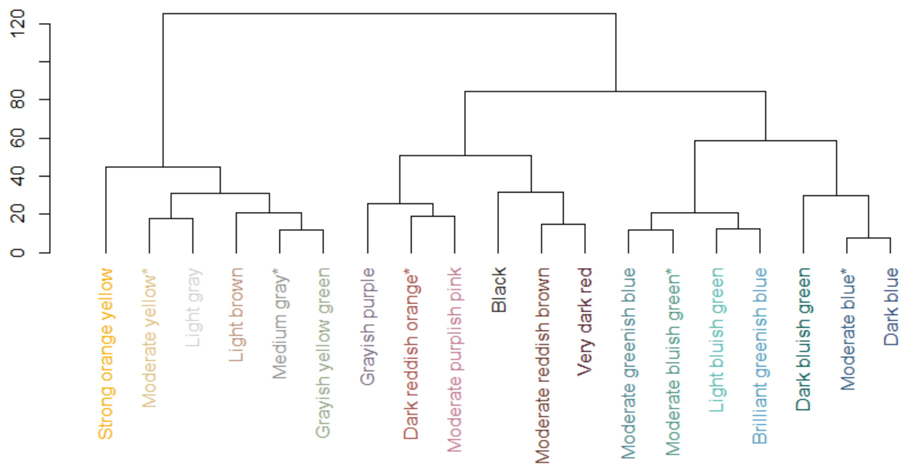

Figure 3.12: Dendrogram for result of hierarchal clustering using the Ward method with distance of the squared KL divergence

On the whole, it's seen that the hierarchical classification with the combination of three types of dendrogram calculation and the translation of KL divergence are well work based on the pattern of color centers.

Therefore, it's seem that color centers and positive definite matrices have the strong relationship.

Chapter 4

Regression analysis of positive definite matrix with log-normal distribution

In this chapter, we construct a regression model between the positive definite matrices and color centers [21]. Recall that $\{(\boldsymbol{u}_i, \boldsymbol{V}_i) \in \mathbb{R}^3 \times \mathcal{V} \mid i = 1, \ldots, n\}$ is the DuPont dataset with a set of positive definite matrices $\mathcal{V}$. In general, $\boldsymbol{V} \in \mathcal{V}$ has the following decomposition based on an orthogonal matrix $\boldsymbol{Q}$ as follows.

$$\boldsymbol{V} = \boldsymbol{Q}\boldsymbol{D}\boldsymbol{Q}^T \tag{4.1}$$

$$\boldsymbol{D} = \begin{pmatrix} \lambda_1 & & \mathbf{0} \\ & \lambda_2 & \\ \mathbf{0} & & \lambda_3 \end{pmatrix}, \quad \lambda_i > 0. \tag{4.2}$$

Then, we define a logarithm of $\boldsymbol{V}$ by

$$\log \boldsymbol{V} = \boldsymbol{Q} \begin{pmatrix} \log \lambda_1 & & \mathbf{0} \\ & \log \lambda_2 & \\ \mathbf{0} & & \log \lambda_3 \end{pmatrix} \boldsymbol{Q}^T. \tag{4.3}$$

Now, we use the log normal regression model[22] described by:

$$\log \boldsymbol{V}_i := \boldsymbol{M}_0 + a_i \boldsymbol{M}_1 + b_i \boldsymbol{M}_2 + L_i \boldsymbol{M}_3 + \boldsymbol{E}_i, \qquad i = 1, 2, \ldots, n \tag{4.4}$$

where $\boldsymbol{M}_j$ $(j = 0, 1, 2, 3)$ are unknown symmetric matrices of order 3 and $n = 19$. They are regression coefficient matrices for explanatory variables

$1, a_i, b_i$ and L_i. We assume that error matrices $\boldsymbol{E}_i$ $(i = 1, 2, ..., n)$ are distributed independently.

Let $\tilde{\boldsymbol{H}} = (\boldsymbol{H}_1, \ldots, \boldsymbol{H}_n)^T : 3n \times 3$ with $\boldsymbol{H}_i = \log \boldsymbol{V}_i$, and $\tilde{\boldsymbol{M}} = (\boldsymbol{M}_0, \ldots, \boldsymbol{M}_3)^T$: 12×3. The design matrix $\boldsymbol{X}$ is set as follows.

$$\boldsymbol{X} = \begin{pmatrix} 1 & a_1 & b_1 & L_1 \\ 1 & a_2 & b_2 & L_2 \\ \vdots & \vdots & \vdots & \vdots \\ 1 & a_n & b_n & L_n \end{pmatrix} : n \times 4. \tag{4.5}$$

Then, the log normal regression model (4.4) is rewritten as

$$\boldsymbol{H}_i = \boldsymbol{M}_0 + a_i \boldsymbol{M}_1 + b_i \boldsymbol{M}_2 + L_i \boldsymbol{M}_3 + \boldsymbol{E}_i \tag{4.6}$$

for $i = 1, 2, \ldots, n$. Thus we have the following simultaneous equation:

$$\tilde{\boldsymbol{H}} \equiv \begin{pmatrix} \boldsymbol{H}_1 \\ \boldsymbol{H}_2 \\ \vdots \\ \boldsymbol{H}_n \end{pmatrix} = \begin{pmatrix} \boldsymbol{I}, & a_1\boldsymbol{I}, & b_1\boldsymbol{I}, & L_1\boldsymbol{I} \\ \boldsymbol{I}, & a_2\boldsymbol{I}, & b_2\boldsymbol{I}, & L_2\boldsymbol{I} \\ \vdots & \vdots & \vdots & \vdots \\ \boldsymbol{I}, & a_n\boldsymbol{I}, & b_n\boldsymbol{I}, & L_n\boldsymbol{I} \end{pmatrix} \begin{pmatrix} \boldsymbol{M}_0 \\ \boldsymbol{M}_1 \\ \boldsymbol{M}_2 \\ \boldsymbol{M}_3 \end{pmatrix} + \begin{pmatrix} \boldsymbol{E}_1 \\ \boldsymbol{E}_2 \\ \vdots \\ \boldsymbol{E}_n \end{pmatrix} \tag{4.7}$$

$$= \tilde{\boldsymbol{X}} \tilde{\boldsymbol{M}} + \tilde{\boldsymbol{E}}. \tag{4.8}$$

The regression coefficient matrix $\tilde{\boldsymbol{M}}$ is estimated by the least square method by minimizing the following error function.

$$\begin{aligned} \operatorname{trace}(\boldsymbol{S}^T \boldsymbol{S}) &= \operatorname{trace}\left(\tilde{\boldsymbol{M}}^T \tilde{\boldsymbol{X}}^T \tilde{\boldsymbol{X}} \tilde{\boldsymbol{M}}\right) - 2\operatorname{trace}\left(\tilde{\boldsymbol{M}}^T \tilde{\boldsymbol{X}}^T \tilde{\boldsymbol{H}}\right) \\ &+ \operatorname{trace}\left(\tilde{\boldsymbol{H}}^T \tilde{\boldsymbol{H}}\right) \end{aligned} \tag{4.9}$$

where

$$\boldsymbol{S} = \tilde{\boldsymbol{H}} - \tilde{\boldsymbol{X}} \tilde{\boldsymbol{M}} \tag{4.10}$$

The derivative of the error function is defined as follow.

$$\frac{\partial \operatorname{trace}(\boldsymbol{S}^T \boldsymbol{S})}{\partial \tilde{\boldsymbol{M}}} = 2\tilde{\boldsymbol{X}}^T \tilde{\boldsymbol{X}} \tilde{\boldsymbol{M}} - 2\tilde{\boldsymbol{X}}^T \tilde{\boldsymbol{H}} = O. \tag{4.11}$$

Then, the regression coefficient matrix is estimated as

$$\widehat{\boldsymbol{M}} = \left\{ \left(\boldsymbol{X}^T \boldsymbol{X} \right)^{-1} \otimes \boldsymbol{I} \right\} \tilde{\boldsymbol{X}}^T \tilde{\boldsymbol{H}} \tag{4.12}$$

$$= \left(\boldsymbol{X}^T \boldsymbol{X} \right)^{-1} \sum_{i=1}^{n} \begin{pmatrix} \boldsymbol{H}_i \\ a_i \boldsymbol{H}_i \\ b_i \boldsymbol{H}_i \\ L_i \boldsymbol{H}_i \end{pmatrix}. \tag{4.13}$$

Thus, $\log \boldsymbol{V}$ at a color point $(a, b, L)^T$ is estimated by

$$\log \hat{\boldsymbol{V}} = \hat{\boldsymbol{M}}_0 + a\hat{\boldsymbol{M}}_1 + b\hat{\boldsymbol{M}}_2 + L\hat{\boldsymbol{M}}_3. \tag{4.14}$$

Then, the positive definiteness of $\hat{\boldsymbol{V}} \equiv \exp\left(\log \hat{\boldsymbol{V}}\right)$ is obviously satisfied because eigenvalues of $\hat{\boldsymbol{V}}$ are positive.

4.1 Numerical experiments though DuPont dataset

Here, the result of the numerical experiment as prediction of ellipsoids by the log-normal regression model though DuPont dataset is shown in Figure 4.1 compared with true case in Figure 4.2.

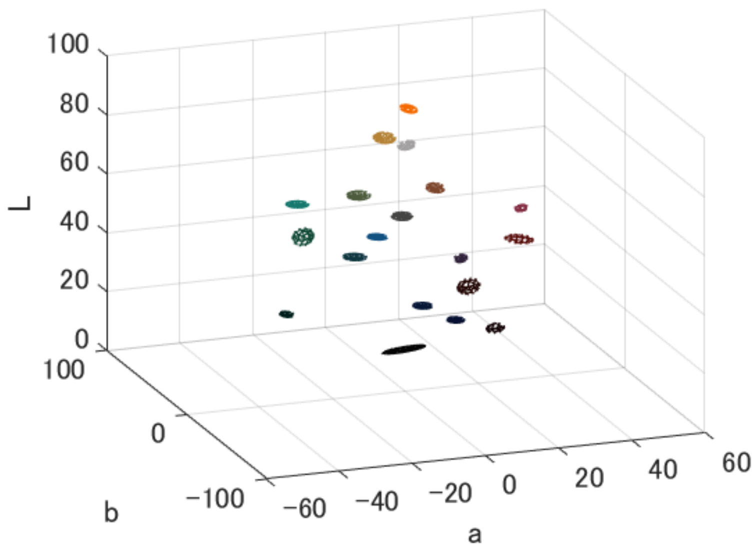

Figure 4.1: Matrix log normal estimation

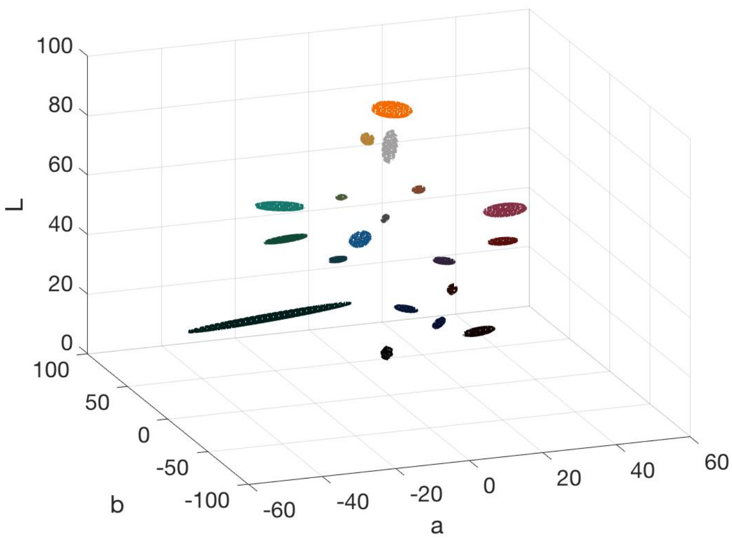

Figure 4.2: True ellipsoids of 19 colors

4.2 Evaluation of prediction methods for positive definite matrix

Table 4.1 compares four optimized models by the DuPont dataset. The second row shows the sum of Frobenius norms between 19 true and estimated matrices by each proposed method. The third and fourth rows are similarly derived by Rimannian and KL metrics. We use the three optimal kernel methods with three bandwidths found in Table 2.3.

Of course, kernel methods based on Frobenius norm gives the minimum Frobenius norm, and so on. The accuracy of log normal regression, however, is poor to kernel methods.

Table 4.1: Evaluation of the estimated results by the three metrics

Evaluation metrics	Estimation methods			
	Non-parametric			Parametric
	Frobenius	Riemannian	Kullback-Leibler	Log normal
Frobenius	**586.78**	641.95	638.65	845.95
Riemannian	21.50	**19.54**	19.60	36.97
Kullback-Leibler	6.40	6.31	**6.29**	16.29

With Figure 2.1 to 2.3 It is seen that all the models failed to estimate the flat-shaped ellipsoid of "Dark bluish green". This may come from the fact that this color is located in the edge of 19 training colors. It is also seen that estimated ellipsoids in (e) by log normal regression are smaller than those by kernel methods in (b)-(d). The log normal regression, however, has an advantage that the linear estimation has a closed form of the solution. Also, the model is easily to implement new explanatory variables such as second-order models.

Chapter 5

Prediction and evaluation of the positive definite matrix for new colors

In this chapter, I will try to apply some prediction methods of positive definite matrices described until previous chapters to the color matching in the automotive appearance design , which are the Kernel estimation methods with combination of three normalizations and three bandwidth tuning parameters, and the regression model having the log-normal distribution of positive definite matrix.

5.1 Color matching in the automotive appearance design

Figure 5.1 depicts illustrations of the color matching target examples in automotive appearance. The color matching targets in this illustrations are combination of parts as following well known.

(a) Bonnet and front bumper.

(b) Bumper and side panel.

(c) Bonnet and fender.

(d) Side panel and front door.

(e) Front and rear door.

(f) Rear door and Rear bumper.

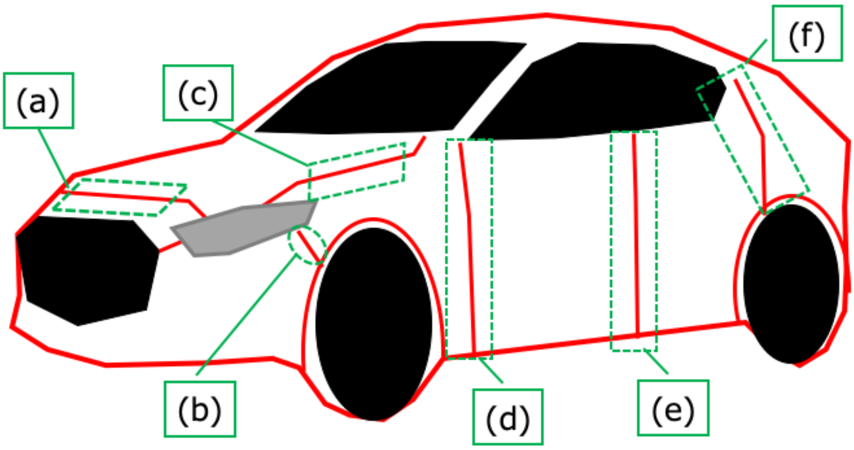

Figure 5.1: Illustrations of the color matching target examples in automotive appearance design

Several pieces is coated on another material, for example the bonnet and side panel are made by steel plate, and the bumper is made by plastic. For that reason, the coating method, pigment quality, and so on are different from each part. However combinations of these pieces must be recognized as same color by user.

It's known that there is measuring equipment of color values $\boldsymbol{u} = (a, b, L)^T$ for appearance evaluation shown in Figure 5.2 , which is constructed by a closed box with a stable light source and multi angle receipt. For example of a equipment's spec as well known, the input angle θ of light source is 45 (deg) with fixed and the receipt angle ϕ has the case of which 45 (deg) called as the mirror reflection, 90 (deg) as the vividness, and 155 (deg) as the shaded area.

As general color matching, $\boldsymbol{u}$ of the referenced master sample is measured by this equipment and putted as color center value $\boldsymbol{u}_c = (a_c, b_c, L_c)^T$. After that, the $\boldsymbol{u}$ of another parts is measured. Finally, the balances of coating materials, the condition of painting robot, and so on are reconfigured so that $\boldsymbol{u} - \boldsymbol{u}_c = 0$. The conventional color matching procedure is to apply these steps above described to all area of vehicle.

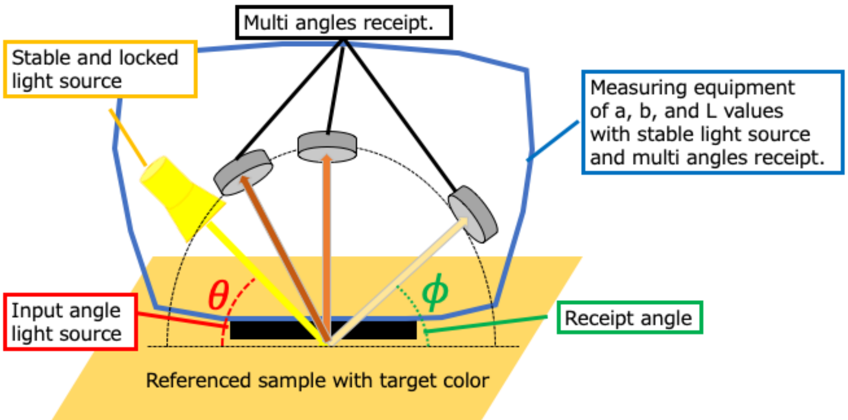

Figure 5.2: Measuring system of color values given as $\boldsymbol{u} = (a, b, L)^T$ in automotive appearance design

It's known that the traditional color matching procedure spends a lot of time in automotive maker, because many parameters resetting of coating materials, painting robot, and so on is mainly realized at painting plant, and some body panels is produced by another plant or implementor. Furthermore, the conventional color matching procedure so that $\boldsymbol{u} - \boldsymbol{u}_c = 0$ make realizing more difficult to achieve, because the latest color trend in the automotive is compatible the vividness and the shading.

Then, I considered that the threshold for judgement of same or not color between parts may be effective based on the human's visual feature.

5.2 Predicted ellipsoids by the proposed methods

Here, I try to predict the positive definite matrix for an actual color in order to show the effectiveness some proposed approaches in previous chapters. Target color centers $\boldsymbol{u}_c = (a_c, b_c, L_c)^T$ is displayed in Table 5.1

corresponding to three receipt angles $\phi = 60$, 90, and 155 (deg). This target color is red with very vivid and a dark shadow because color center values at the receipt angle $\phi = 60$ (deg) are large and them at $\phi = 90$ and 155 (deg) are very small.

Table 5.1: Dataset of a actual color values

ϕ(deg.)	a_c	b_c	L_c
60	84.54	78.17	42.29
90	25.42	10.20	5.31
155	19.30	5.82	3.75

I predict ellipsoids of color centers corresponding to three receipt angles shown in Table 5.1 by following four methods.

(i) Prediction of positive definite matrices by applying three bandwidth tuning parameters $\gamma_F = 200.1$, $\delta_F = 1.25$, and $\eta_F = 1.813$ shown in Table 2.3 with combination of the Frobenius norm and normalization method 2 , and color center values shown in Table 5.1 , to (2.26), (2.27), and (2.28).

(ii) Prediction of positive definite matrices by applying three bandwidth tuning parameters $\gamma_R = 36.78$, $\delta_R = 15.81$, and $\eta_R = 17.13$ shown in Table 2.3 with combination of the Riemannian metric and normalization method 3 , and color center values shown in Table 5.1 , to (2.26), (2.27), and (2.28).

(iii) Prediction of positive definite matrices by applying three bandwidth tuning parameters $\gamma_{KL} = 44.59$, $\delta_{KL} = 18.50$, and $\eta_{KL} = 21.00$ shown in Table 2.3 with combination of the KL divergence and normalization method 2 , and color center values shown in Table 5.1 , to (2.26), (2.27), and (2.28).

(iv) Prediction by the regression model of positive definite matrix with log-normal distribution by estimating regression coefficient matrices with all 19 colors data of the DuPont dataset.

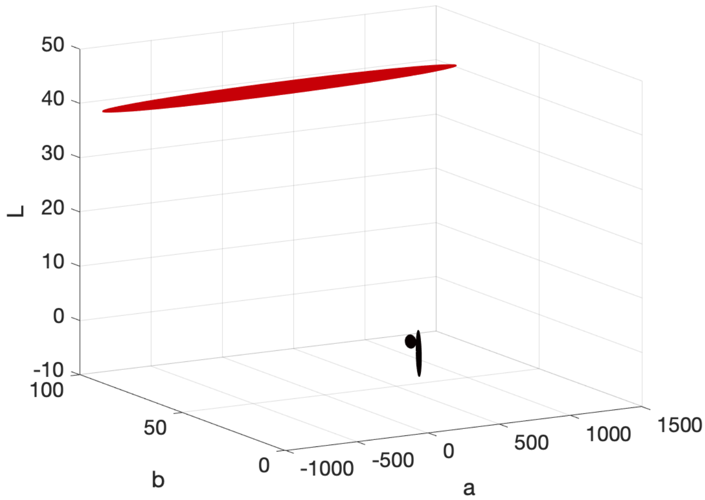

Figure 5.3: Predicted ellipsoids by method **(i)**

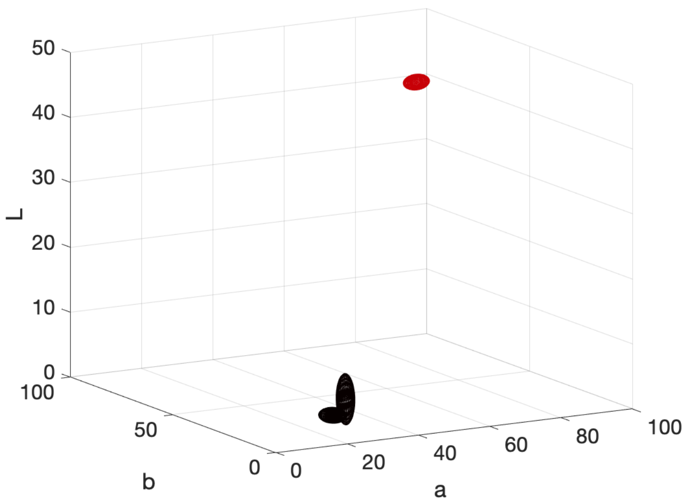

Figure 5.4: Predicted ellipsoids by method **(ii)**

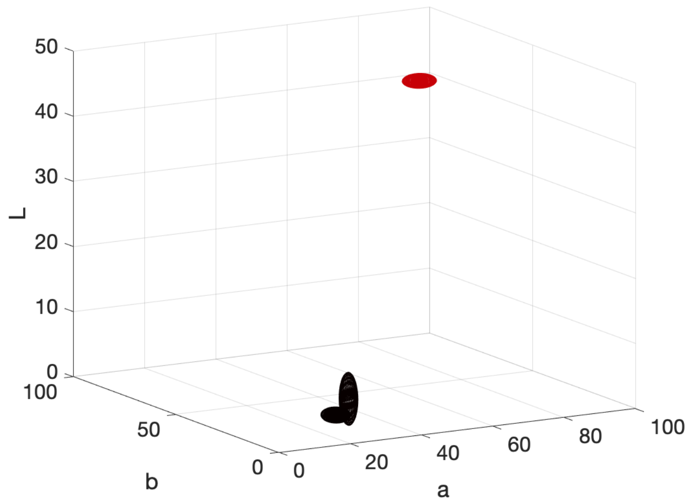

Figure 5.5: Predicted ellipsoids by method **(iii)**

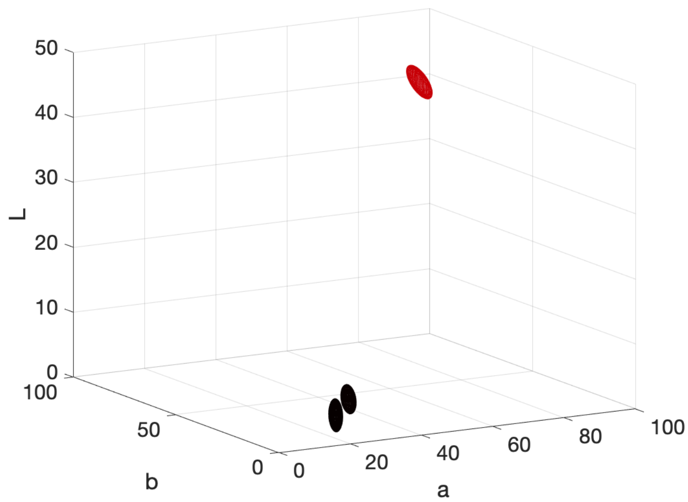

Figure 5.6: Predicted ellipsoids by method **(iv)**

The ellipsoid at receipt angle 60 (deg) predicted by method **(i)** has long shape for direction of a in Figure 5.3 because the $\gamma_F = 200.1$ displayed at

8th row and 9th column in Table 2.3 is largest of all γ_F, which is the bandwidth tuning parameter corresponding to v_{11} of positive definite matrix (2.2).

On the other hand, ellipsoids predicted by method (ii) and (iii) seem to be similar for all receipt angles because three tuning parameters are near shown in Figure 5.4 and 5.5.

Ellipsoids predicted by method (iv) have different shape from previous three methods (Figure 5.6), finally.

5.3 Evaluation of predicted ellipsoids

I will compare to the measured data in Figure 5.7 to 5.10 in order to confirm the effectiveness of each predicted ellipsoids. Measured data was judged as accept by color matching evaluators , and each point had different coating conditions and was measured by equipment in Figure 5.2.

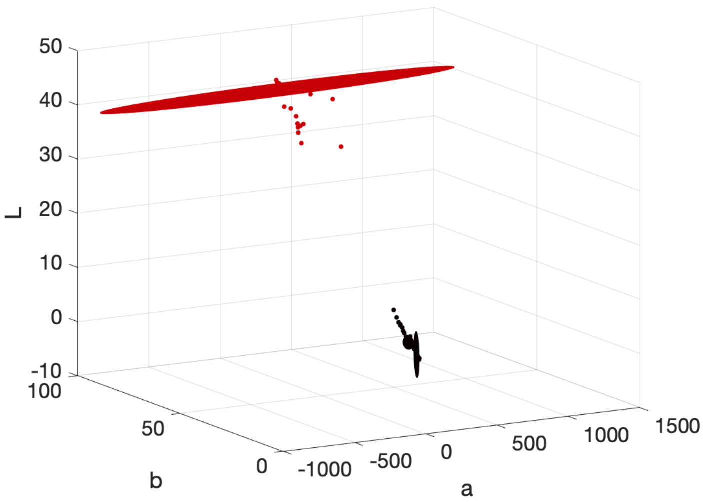

Figure 5.7: Predicted ellipsoids by method **(i)** and measured data.

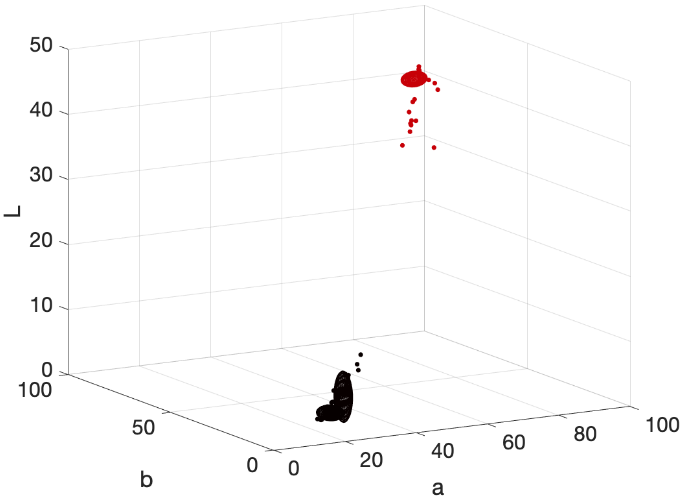

Figure 5.8: Predicted ellipsoids by method **(ii)** and measured data.

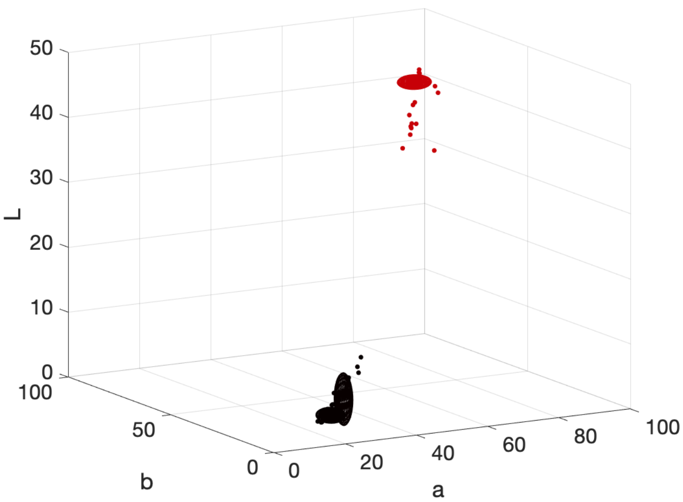

Figure 5.9: Predicted ellipsoids by method **(iii)** and measured data.

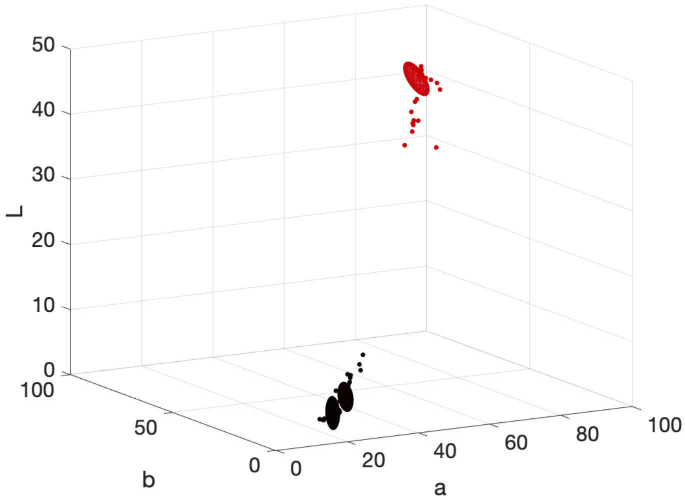

Figure 5.10: Predicted ellipsoids by method **(iv)** and measured data.

It's seen that measured data trends toward a certain direction at the receipt angles 60 and 90 (deg), especially. In the case of receipt angle 60 (deg), ellipsoid predicted by method (iv) is like to be more fit in measured data than other methods. In the case of receipt angle 90 and 155 (deg), ellipsoids predicted by method (ii) and (iii) are like to be more fit in measured data than other methods.

As a result, I consider to have to separate the use of methods , for example , the log - normal regression model in area with large color center values and the Gaussian kernel estimation with small color center values.

Chapter 6

Conclusion

It is known that each color has an ellipsoid region whose points are visually recognized as the same color. Now, the DuPont dataset provides pairs of colors and ellipsoids in CIE-Lab system. Of course, the shape of ellipsoid is determined by a positive definite matrix. Therefore, we have proposed the estimation methods of ellipsoids with a new color center in Lab system.

Firstly, we consider Gaussian kernel estimation of positive definite matrices with three bandwidths at most and three types of normalization methods of explanatory variables. The third as well as second normalization methods work well for estimation. The bandwidths were tuned by minimizing the three metrics Frobenius, Riemmanian, and KL. Three metrics show similar performance for estimation. It is noted that this weighted-sum approach has a theoretical justification based on KL divergence.

Secondly, we used the matrix-valued log normal regression. This approach has the closed solution for regression coefficient matrices, and gives an ellipsoid of a new color easily. Unfortunately, this shows a poor performance with respect to kernel estimation. This may be improved by using additional explanatory variables derived by color features.

The paint shop of the automotive manufacturer needs more than one month to adjust the painting condition for synthesis of the same color. On the other hand, the color matching admitting tolerant ellipsoid would be easily tuned within one week because the painting condition of robot painters can be configured applying tolerance ellipsoids. This would make possible to mass-produce new colors with stable quality at factories around the world.

Furthermore, if the human color sensitivity can be modeled, synthesis of new colors would be developed by simulation. We plan to establish a fundamental technology enabling the efficient management of attractive new colors by developing more accurate prediction algorithms based on mathematical approaches. For example, on support vector regression and other approximation techniques as well as on a database of colors and ellipsoids.

Acknowledgments

This research was supported by Mazda Motor Corporation and Grant-in-Aid for Scientific Research(B) 15H02670. The authors are very grateful to two reviewers. Their constructive comments were very helpful to improve the draft drastically. Also, they would like to express for their hearty thanks to the editor for kind handling of the paper.

Bibliography

[1] D. L. MacAdam. Color Measurement Theme and Variations Second Revised Edition. Springer-Verlag, 2nd edition, 1985.

[2] G. A. Agoston. Color Theory and Its Application in Art and Design Second Completely Revised and Updated Edition. Springer-Verlag, 2nd edition, 1987.

[3] J. P. Homann. Digital Color Management. Springer, 2007.

[4] M. R. Luo, G. Cui, and B. Rigg. The development of the cie 2000 colour-difference formula: Ciede2000. COLOR res., 26(5): 340 – 350, 2001.

[5] R. S. Berns and B. Hou. Rit-dupont supra - threshold color - tolerance individual color - difference pair dataset . COLOR res., 35(4): 274 – 283, 2010.

[6] M. Huang, H. Liu, G. Cui, and M. R. Luo. Testing uniform colour spaces and colour - difference formulae using printed samples . COLOR res., 37(5):326 – 335, 2012.

[7] S. Shen and R. S. Berns. Evaluating color difference equation performance incorporating visual uncertainty. COLOR res., 34(5): 375 – 390, 2009.

[8] M. Melgosa, E. Hita, A. J. Poza, D. H. Alman , and R. S. Berns. Suprathreshold color-difference ellipsoid for surface colors. COLOR res. , 22(3): 148 – 155, 1997.

[9] G. M. Johnson and M. D. Fairchild. A top down description of s-cielab and ciede2000. COLOR res., 28(6): 425 – 435, 2003.

[10] R. Shamey, J. Lin,W. Sawatwarakul, and R. Cao. Evaluation of performance of various color-difference formulae using an experimental black dataset. COLOR res. , 39(6):589 – 598, 2014.

[11] S. Zhu, K. Yu, and Y. Gong. Predictive matrix - variate t models. Adv. in Neu, Inf. Proc. Sys, 20, 2007. 2

[12] F. Hiai and D. Petz. Riemannian metrics on positive definite matrices related to means. Linear Algebra and its App., 430:3105 – 3130, 2009.

[13] J. Wu. Advances in K-means Clustering A Data Mining Thinking. Springer, 2012.

[14] J. A. Hartigan and M. A. Wong. A k - means clustering algorithm. J. the Royal Stat. Society. Series C, 28(1):100 – 108, 1979.

[15] M. Moakher. A differential geometric approach to the geometric mean of symmetric positive - definite matrices. SIAM J. Matrix Anal., 26(3): 735 – 747, 2005.

[16] T. Hastie, R. Tibshirani, and J. Friedman. The Elements of Statistical Learning Data Mining, Inference, and Prediction. Springer, 2013.

[17] F. Murtagh and P. Legendre. Ward ' s hierarchical clustering method: clustering criterion and agglomerative algorithm. Journal of Class., 31(3): 274 – 295, 2014.

[18] J. H. Ward Jr. Hierarchical grouping to optimize an objective function. Journal of the American Statistical Association , 58(301):236 – 244, 1963.

[19] J. Fan, N. E. Heckman, and M. P. Wand. Local polynomial kernel regression for generalized linear models and quasi - likelihood functions. Journal of the American Statistical Association, 90(429) : 141 – 150, 1995.

[20] W. S. Cleveland and S. J. Delvin. Locally weighted regression: An approach to regression analysis by local fitting. Journal of the American Statistical Association , 83(403):596 – 610, 1988.

[21] Y. Yuan, H. Zhu, W. Lin, and J. S. Marron. Local polynomial regression for symmetric positive definite matrices. Stat. Methodology, 74(4), 2012.

[22] A. Schwartzman. Lognormal distributions and geometric averages of symmetric positive definite matrices. International Stat. Rev. , 84(3): 456 - 486, 2016.

52

Appendix A

Calcuration results of three types of metric

A.1 Frobenius norm results for three types of bandwidth tuning parameter and normalizarion method

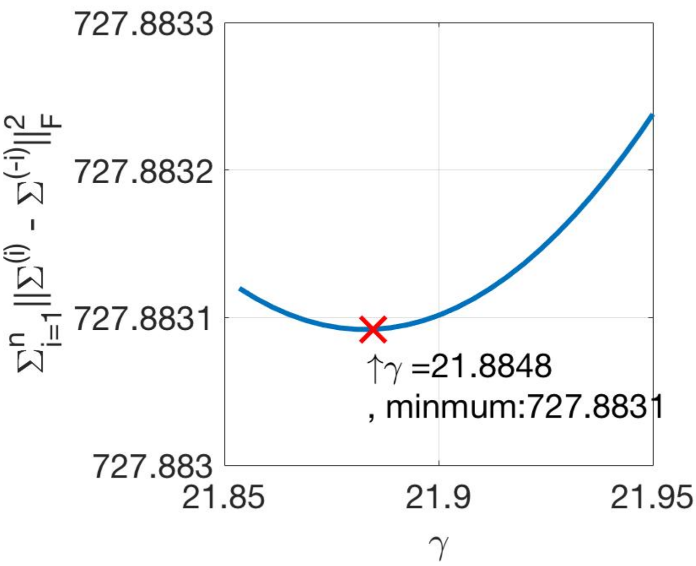

Figure A.1: Frobenius norm result at a single bandwidth tuning parameter with the first normalizarion method.

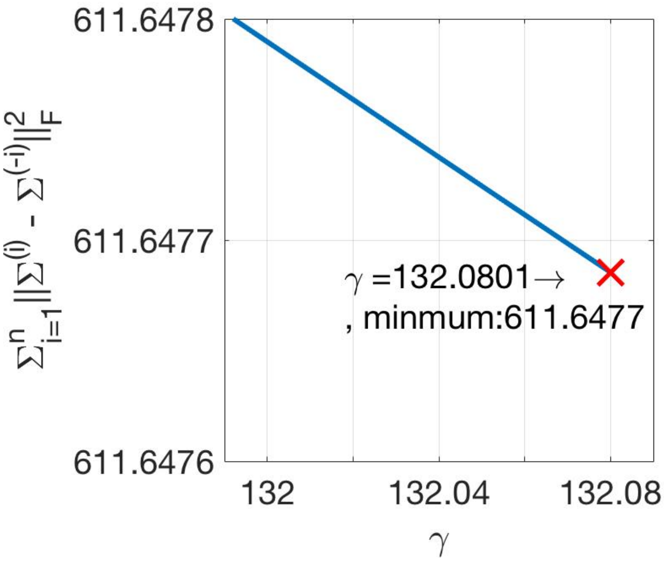

Figure A.2: Frobenius norm result at a single bandwidth tuning parameter with the second normalizarion method.

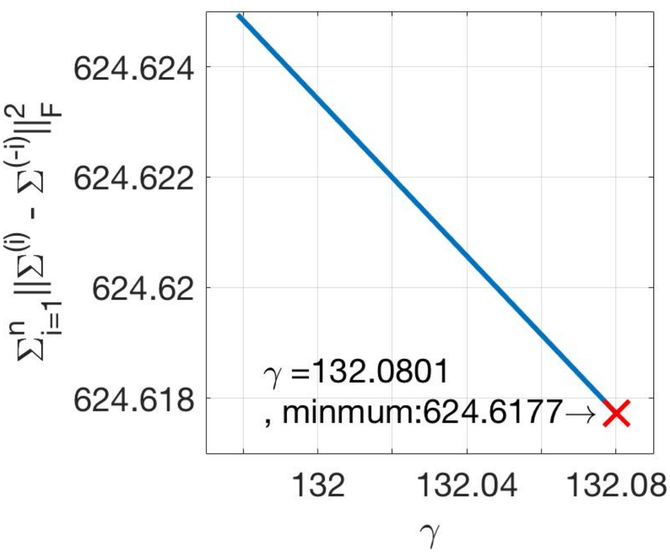

Figure A.3: Frobenius norm result at a single bandwidth tuning parameter with the third normalizarion method.

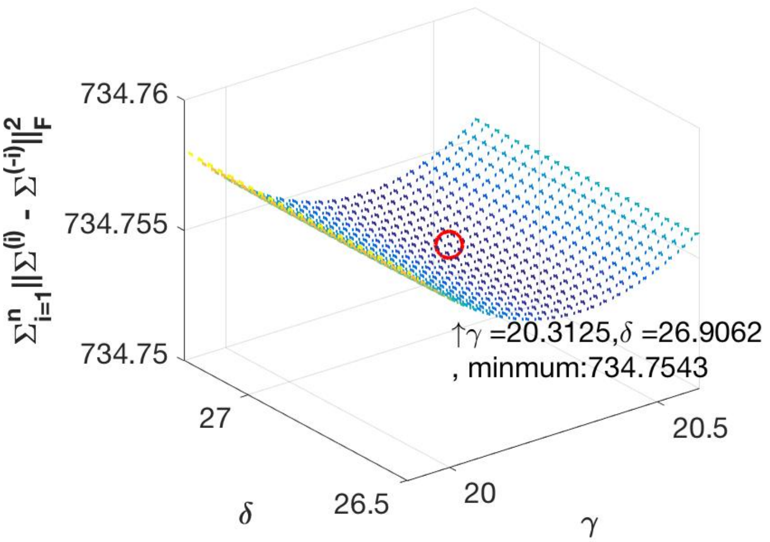

Figure A.4: Frobenius norm result at double bandwidth tuning parameters with the first normalizarion method.

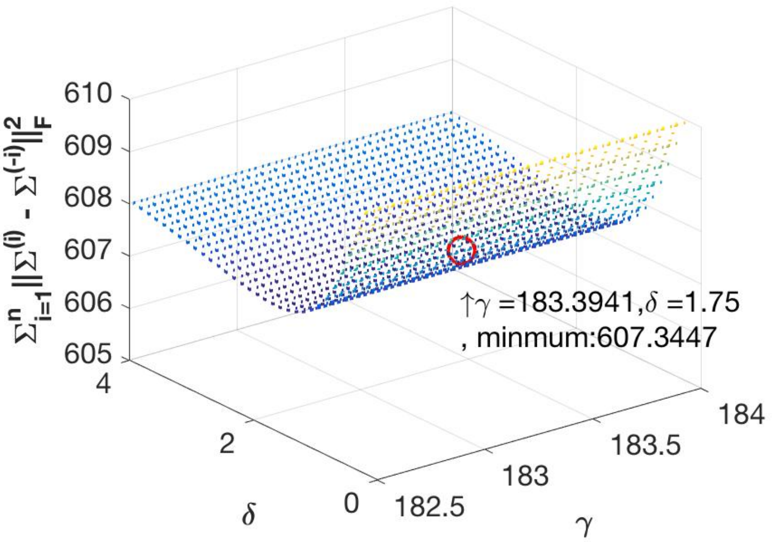

Figure A.5: Frobenius norm result at double bandwidth tuning parameters with the second normalizarion method.

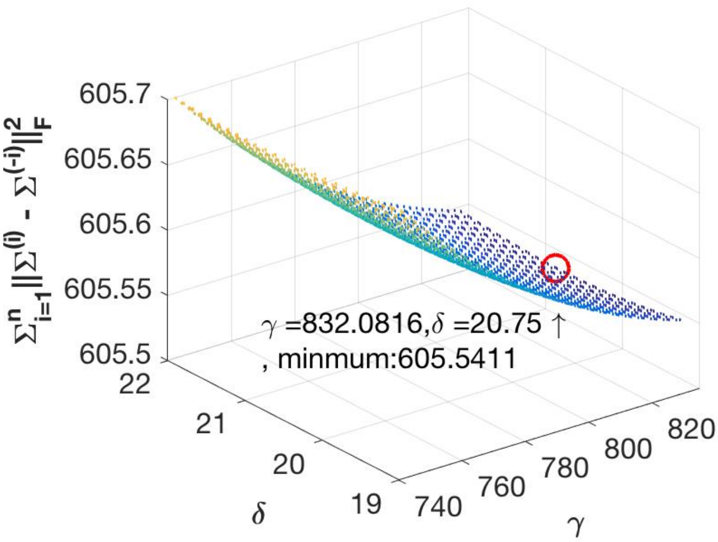

Figure A.6: Frobenius norm result at double bandwidth tuning parameters with the third normalizarion method.

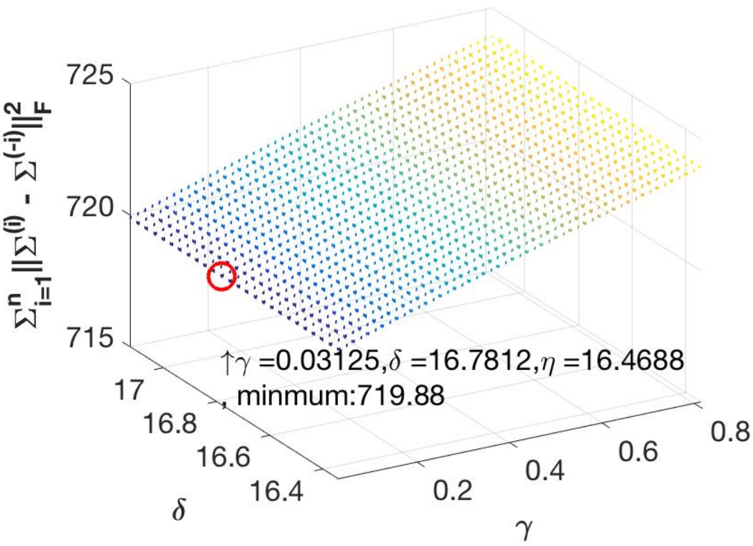

Figure A.7: Frobenius norm result at triple bandwidth tuning parameters with the first normalizarion method.

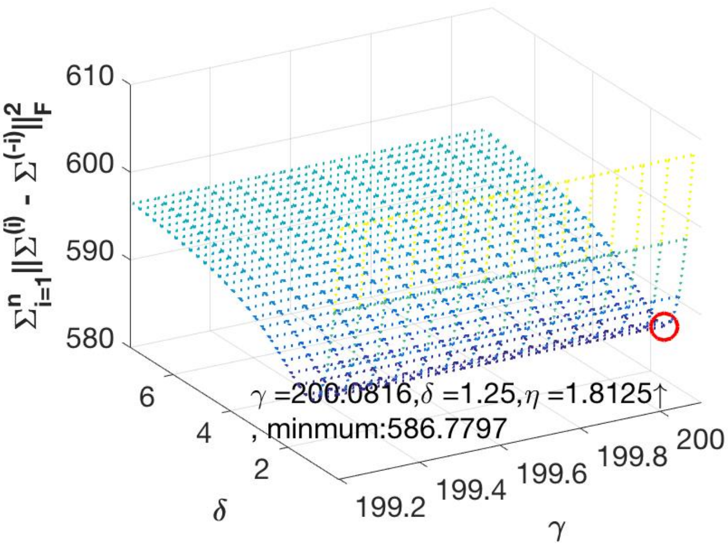

Figure A.8: Frobenius norm result at triple bandwidth tuning parameters with the second normalizarion method.

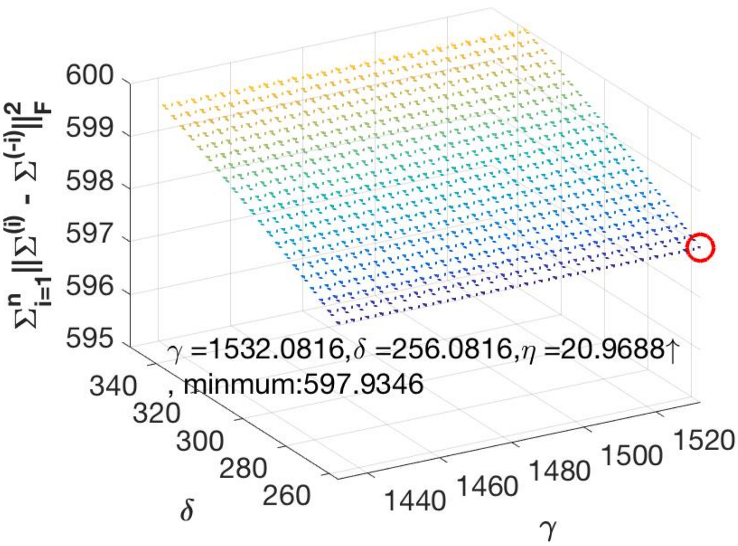

Figure A.9: Frobenius norm result at triple bandwidth tuning parameters with the third normalizarion method.

A.2 Riemannian metric results for three types of bandwidth tuning parameter and normalizarion method

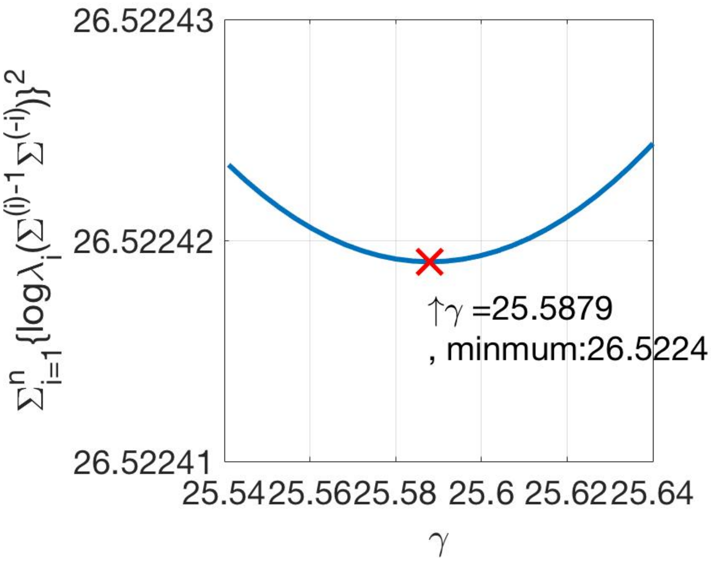

Figure A.10: Riemannian metric result at a single bandwidth tuning parameter with the first normalizarion method.

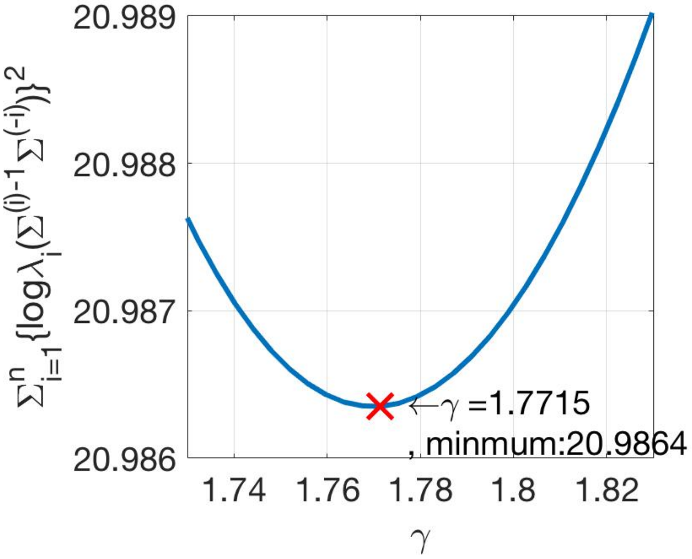

Figure A.11: Riemannian metric result at a single bandwidth tuning parameter with the second normalizarion method.

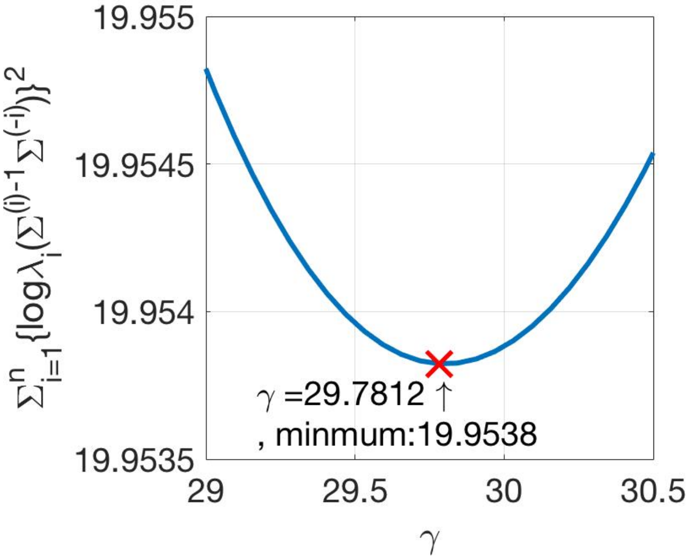

Figure A.12: Riemannian metric result at a single bandwidth tuning parameter with the third normalizarion method.

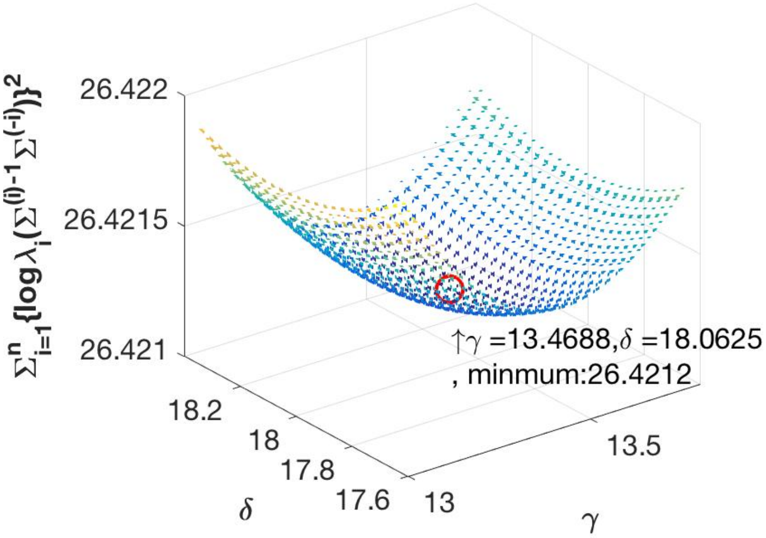

Figure A.13: Riemannian metric result at double bandwidth tuning parameters with the first normalizarion method.

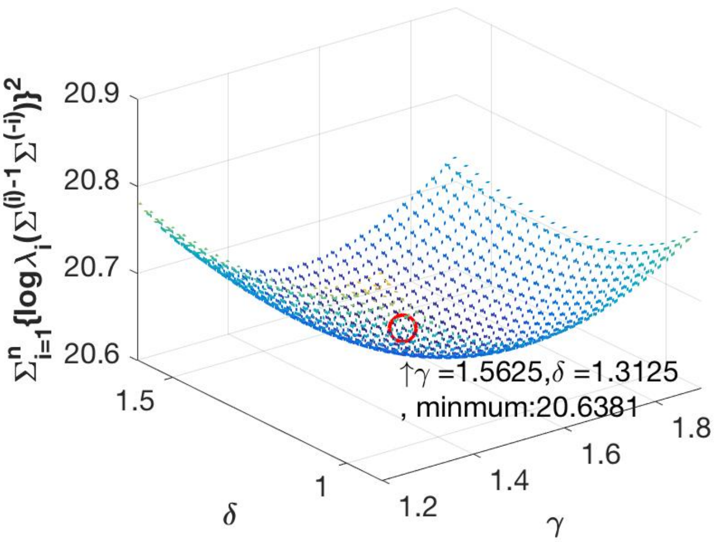

Figure A.14: Riemannian metric result at double bandwidth tuning parameters with the second normalizarion method.

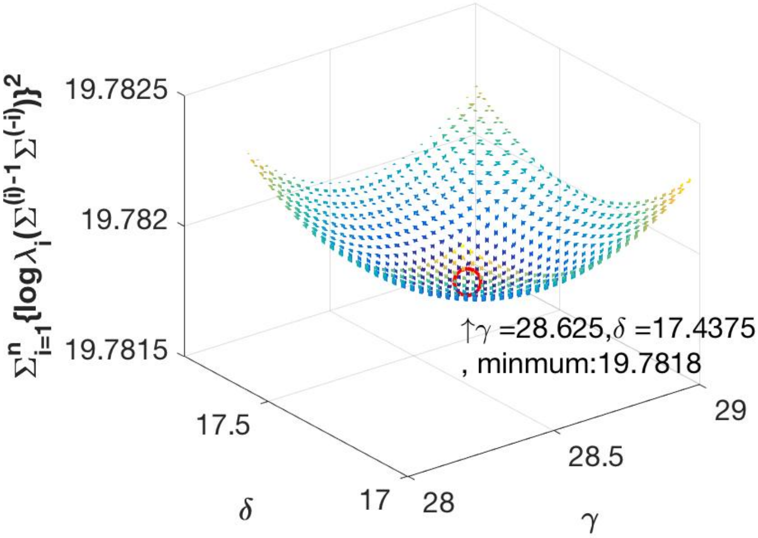

Figure A.15: Riemannian metric result at double bandwidth tuning parameters with the third normalizarion method.

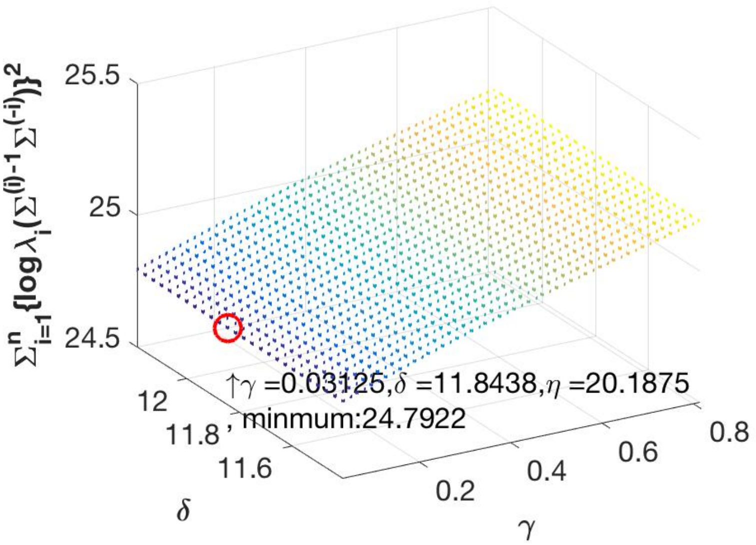

Figure A.16: Riemannian metric result at triple bandwidth tuning parameters with the first normalizarion method.

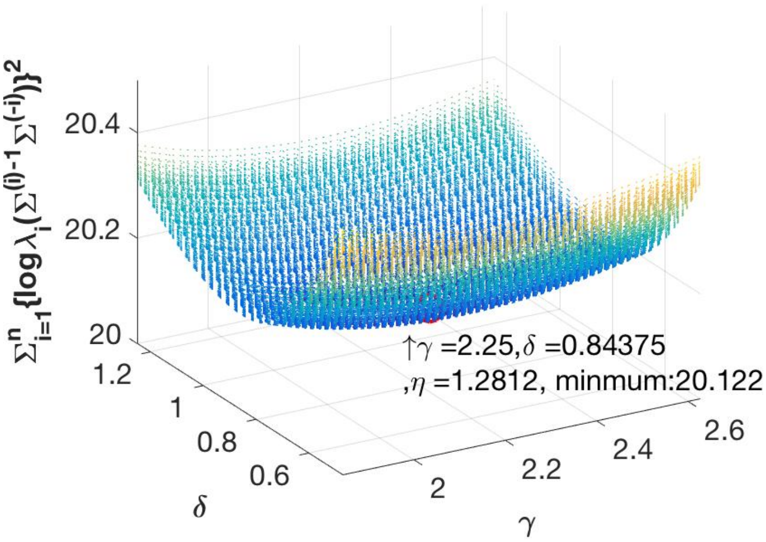

Figure A.17: Riemannian metric result at triple bandwidth tuning parameters with the second normalizarion method.

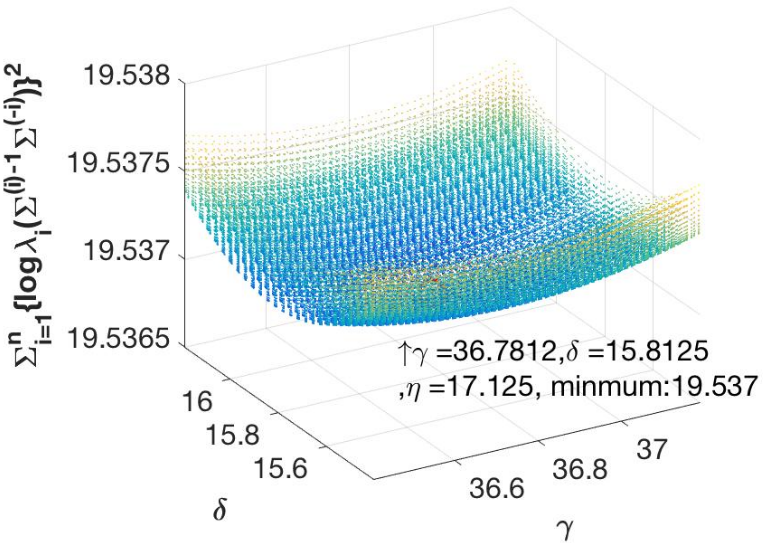

Figure A.18: Riemannian metric result at triple bandwidth tuning parameters with the third normalizarion method.

A.3 KL divergence results for three types of bandwidth tuning parameter and normalizarion method

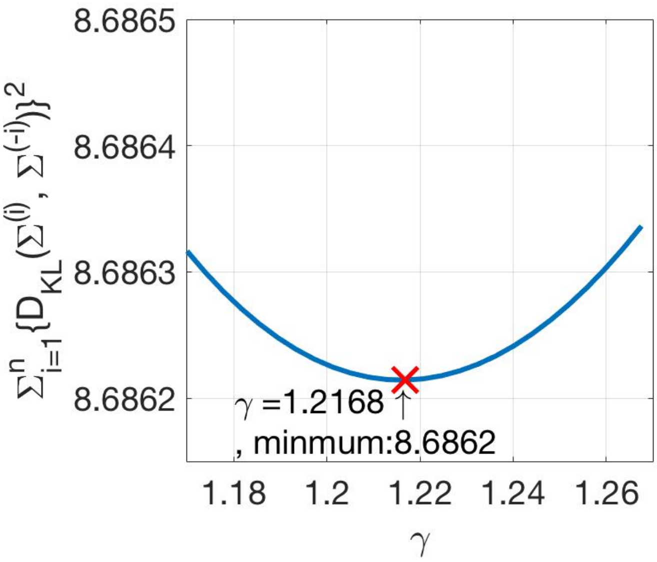

Figure A.19: KL divergence result at a single bandwidth tuning parameter with the first normalizarion method.

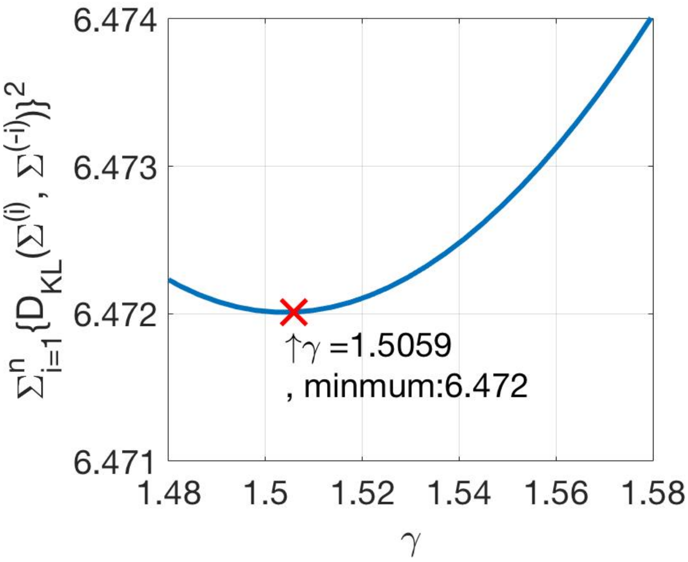

Figure A.20: KL divergence result at a single bandwidth tuning parameter with the second normalizarion method.

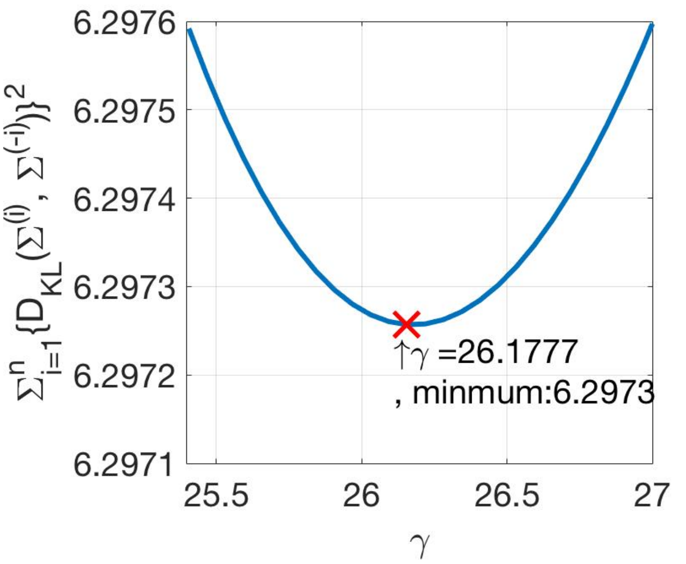

Figure A.21: KL divergence result at a single bandwidth tuning parameter with the third normalizarion method.

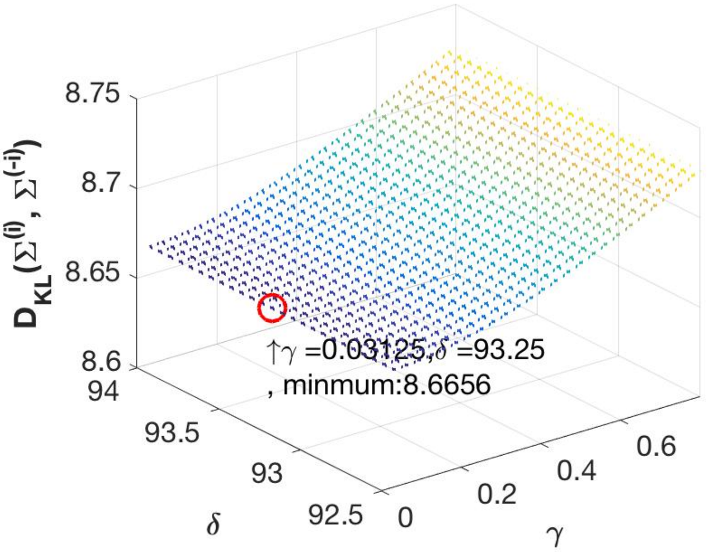

Figure A.22: KL divergence result at double bandwidth tuning parameters with the first normalizarion method.

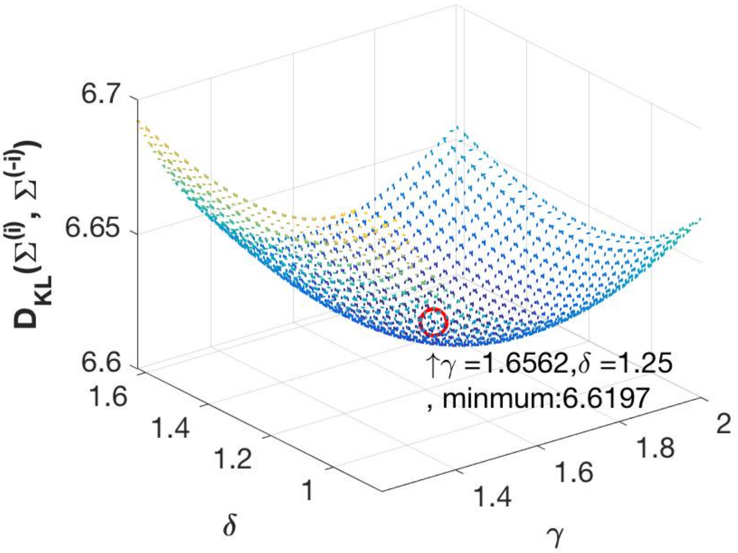

Figure A.23: KL divergence result at double bandwidth tuning parameters with the second normalizarion method.

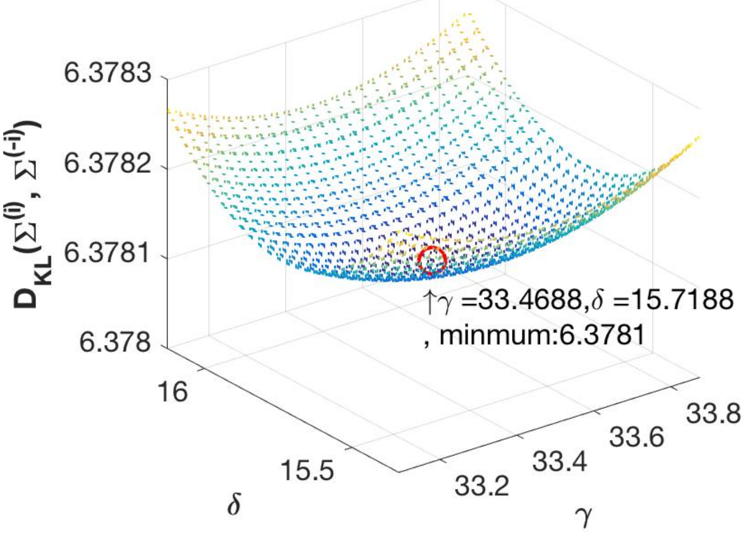

Figure A.24: KL divergence result at double bandwidth tuning parameters with the third normalizarion method.

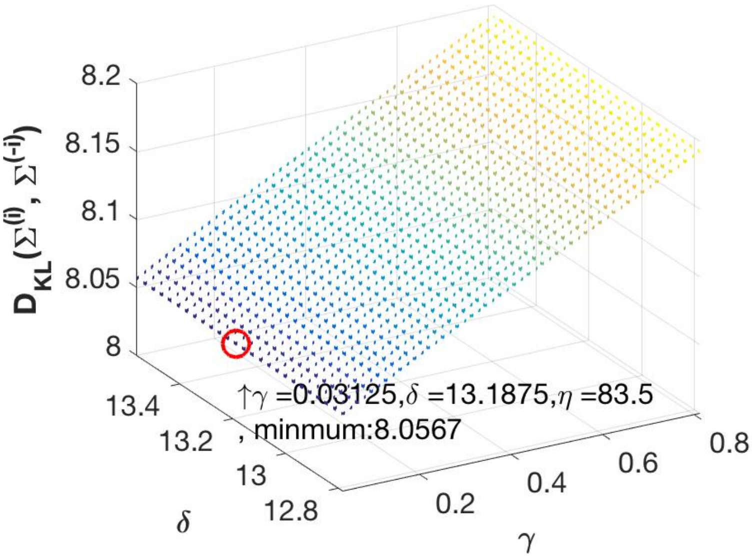

Figure A.25: KL divergence result at triple bandwidth tuning parameters with the first normalizarion method.

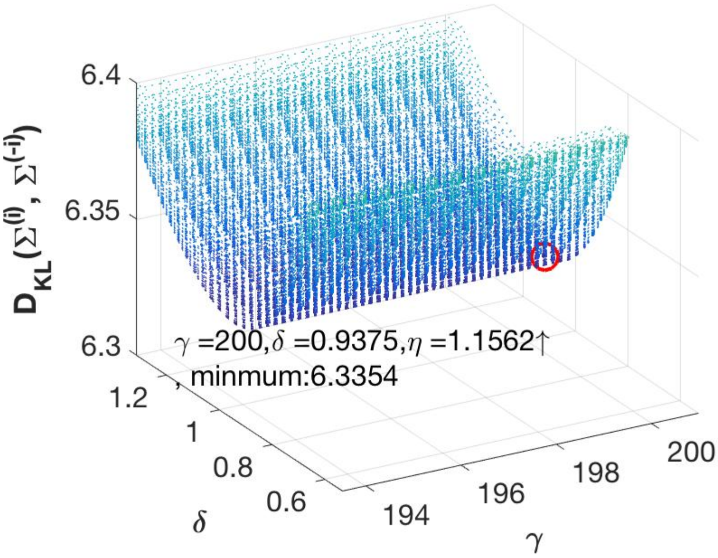

Figure A.26: KL divergence result at triple bandwidth tuning parameters with the second normalizarion method.

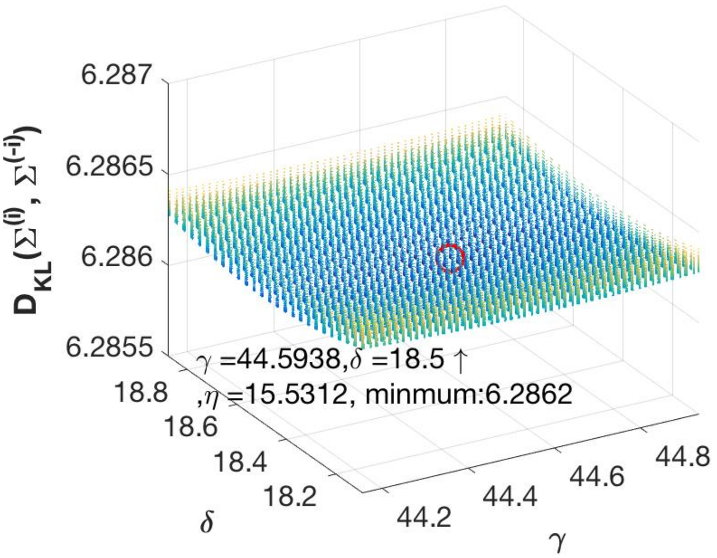

Figure A.27: KL divergence result at triple bandwidth tuning parameters with the third normalizarion method.

Appendix B

Estimated ellipsoids by three types of metric

B.1 Estimation results of ellipsoids with combination of the single bandwidth tuning parameter minimized by the Frobenius norm and three normalization methods

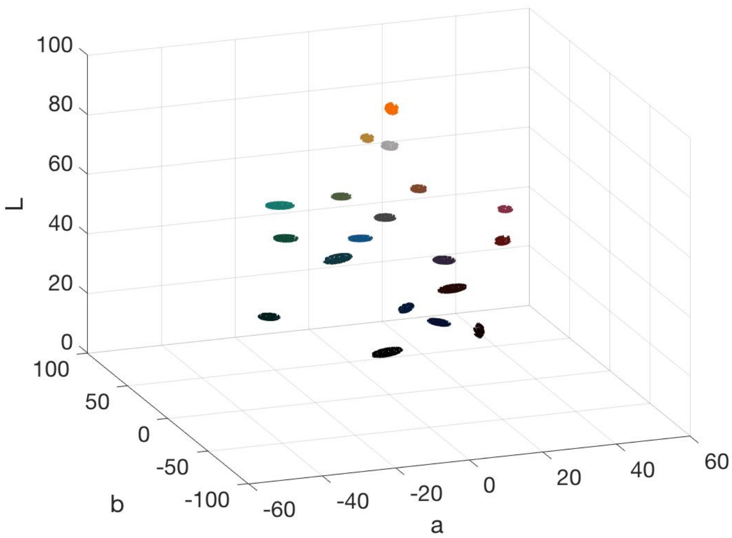

Figure B.1: Estimation of ellipsoids for single bandwidth tuning parameter with the first normalizarion method.

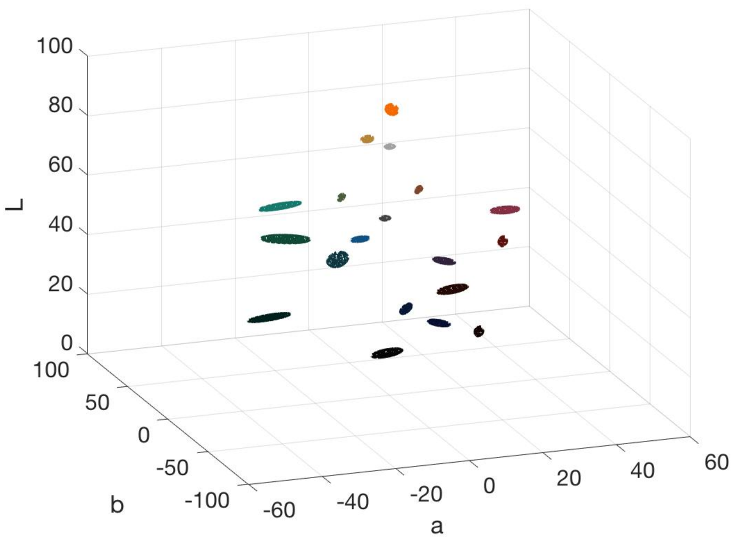

Figure B.2: Estimation of ellipsoids for single bandwidth tuning parameter with the second normalizarion method.

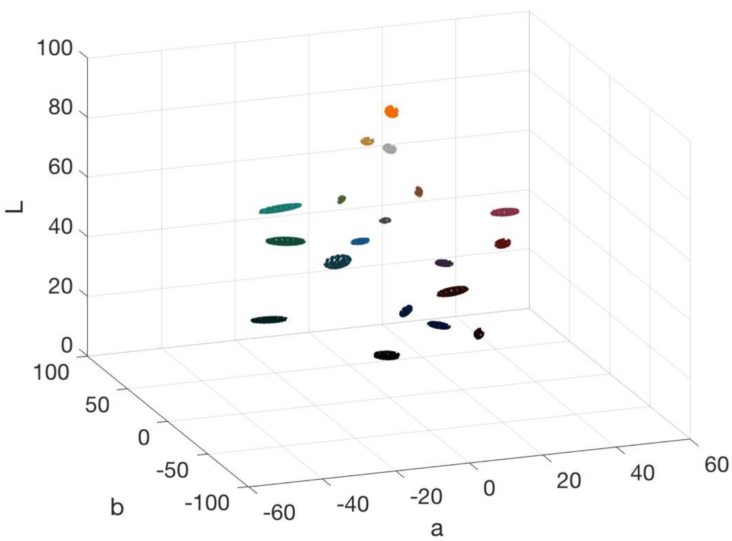

Figure B.3: Estimation of ellipsoids for single bandwidth tuning parameter with the third normalizarion method.

B.2 Estimation results of ellipsoids with combination of the double bandwidth tuning parameters minimized by the Frobenius norm and three normalization methods

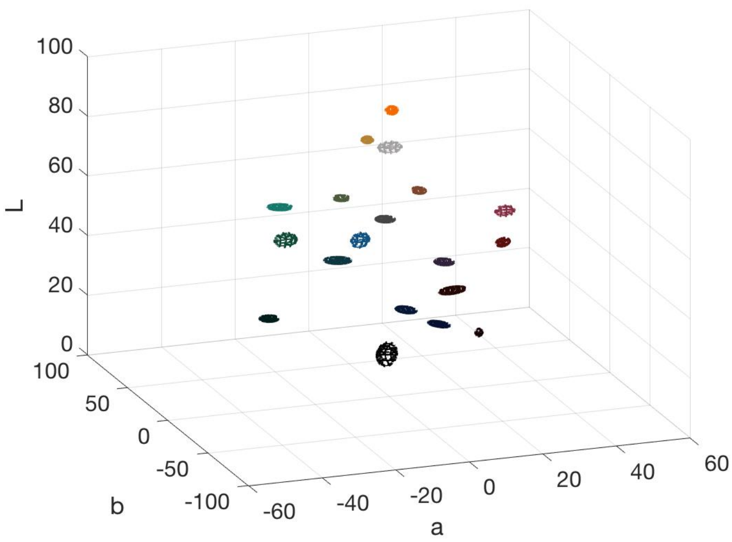

Figure B.4: Estimation of ellipsoids for double bandwidth tuning parameters with the first normalizarion method.

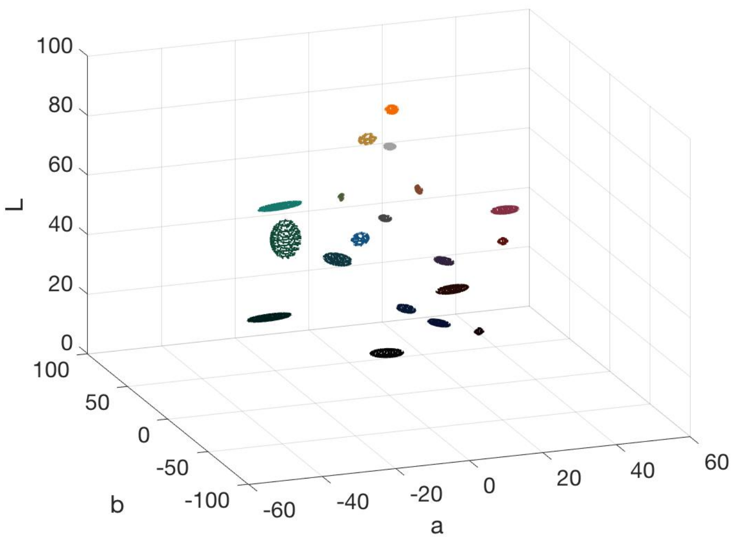

Figure B.5: Estimation of ellipsoids for double bandwidth tuning parameters with the second normalizarion method.

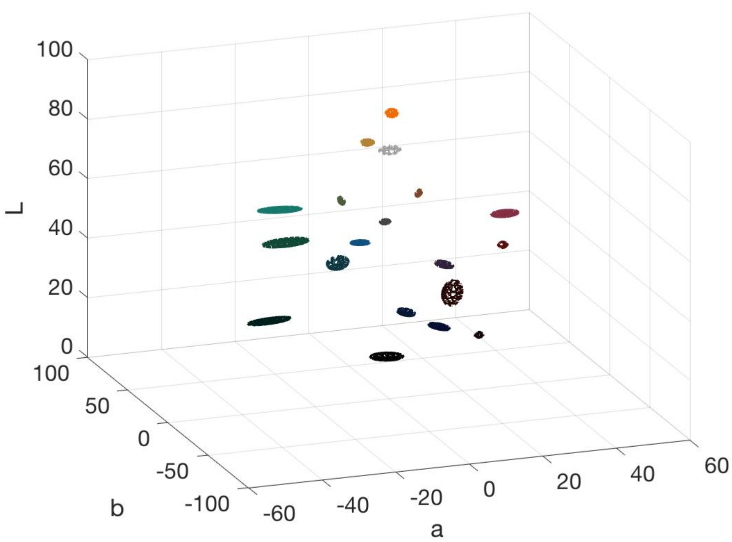

Figure B.6: Estimation of ellipsoids for double bandwidth tuning parameters with the third normalizarion method.

B.3 Estimation results of ellipsoids with combination of the triple bandwidth tuning parameters minimized by the Frobenius norm and three normalization methods

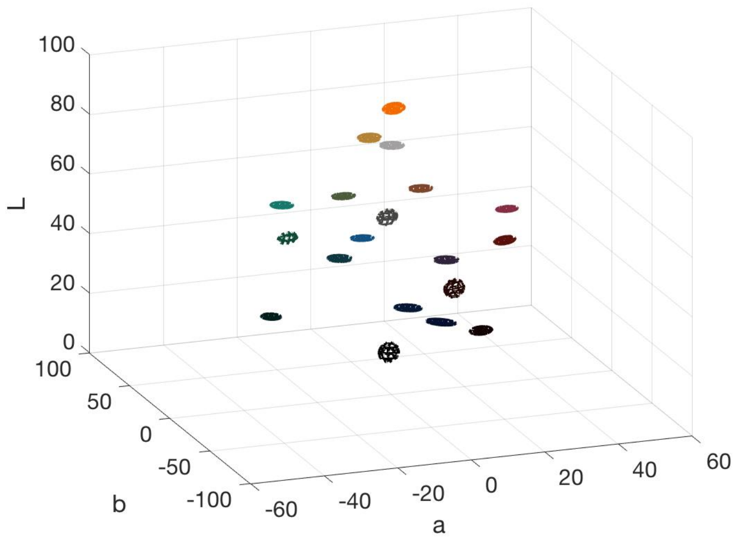

Figure B.7: Estimation of ellipsoids for triple bandwidth tuning parameters with the first normalizarion method.

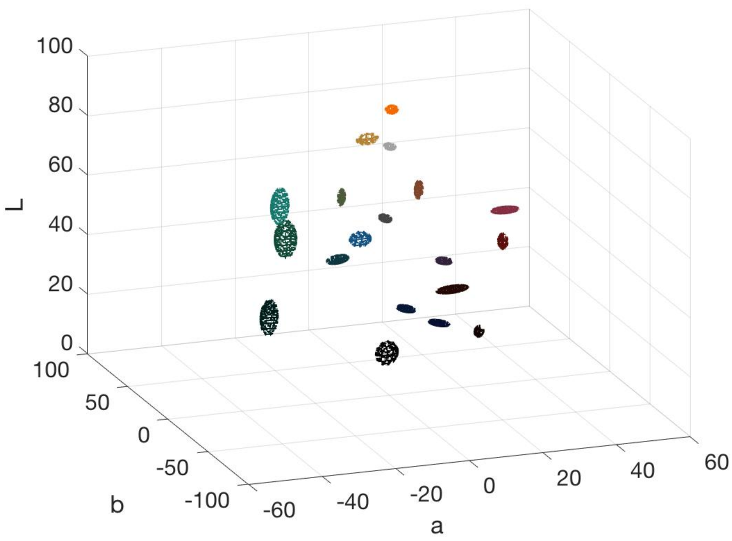

Figure B.8: Estimation of ellipsoids for triple bandwidth tuning parameters with the second normalizarion method.

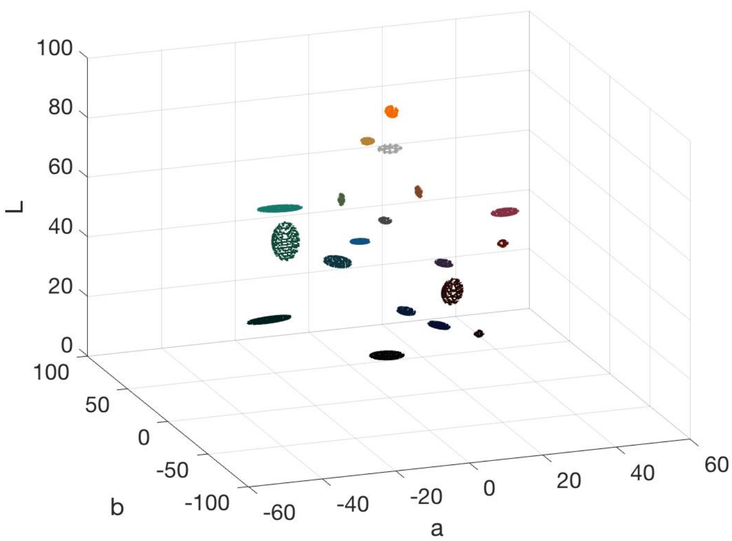

Figure B.9: Estimation of ellipsoids for triple bandwidth tuning parameters with the third normalizarion method.

B.4 Estimation results of ellipsoids with combination of the single bandwidth tuning parameter minimized by the Riemannian metric and three normalization methods

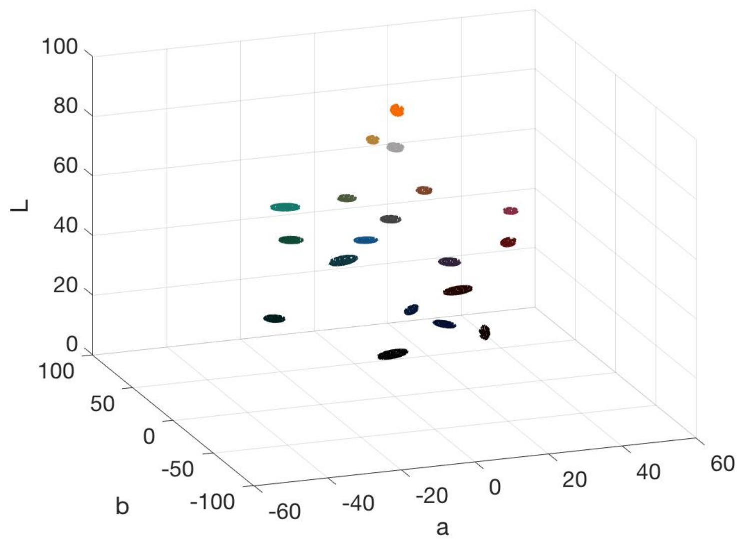

Figure B.10: Estimation of ellipsoids for single bandwidth tuning parameter with the first normalizarion method.

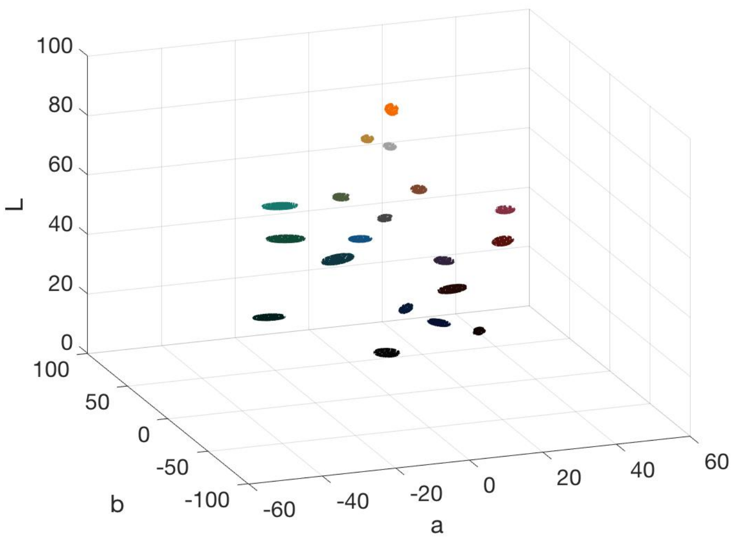

Figure B.11: Estimation of ellipsoids for single bandwidth tuning parameter with the second normalizarion method.

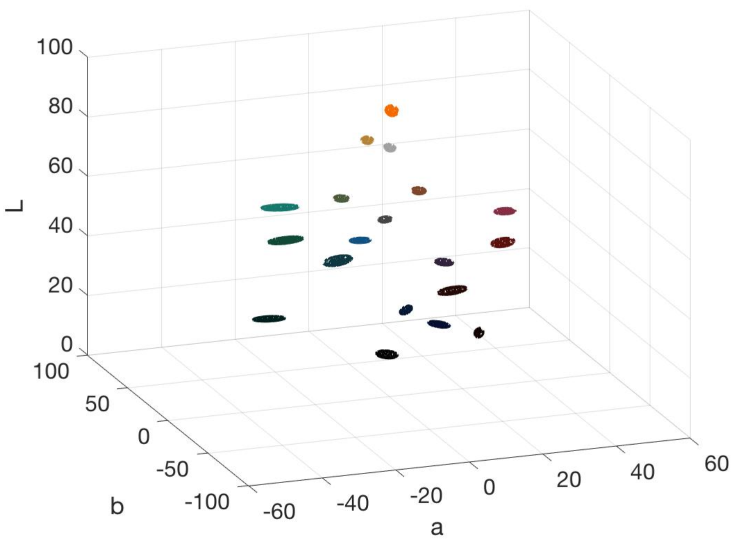

Figure B.12: Estimation of ellipsoids for single bandwidth tuning parameter with the third normalizarion method.

B.5 Estimation results of ellipsoids with combination of the double bandwidth tuning parameters minimized by the Riemannian metric and three normalization methods

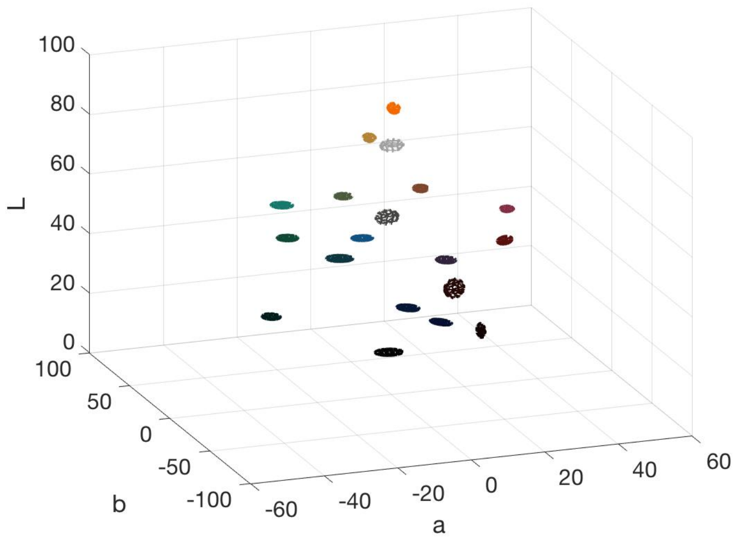

Figure B.13: Estimation of ellipsoids for double bandwidth tuning parameters with the first normalizarion method.

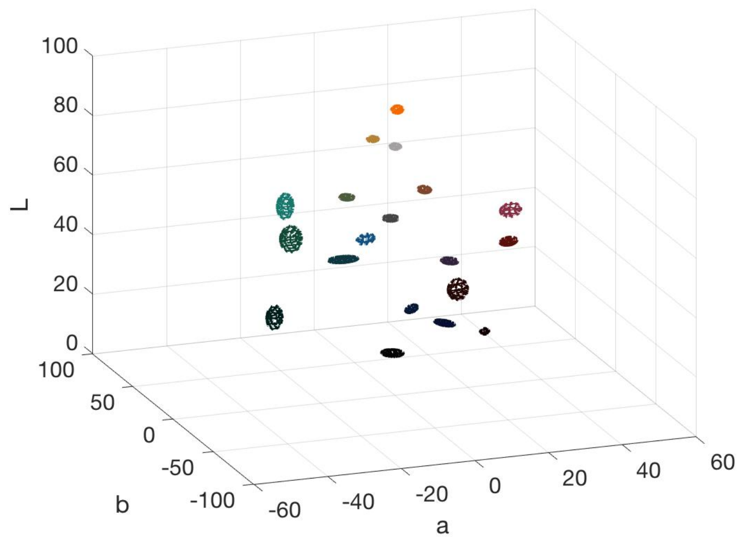

Figure B.14: Estimation of ellipsoids for double bandwidth tuning parameters with the second normalizarion method.

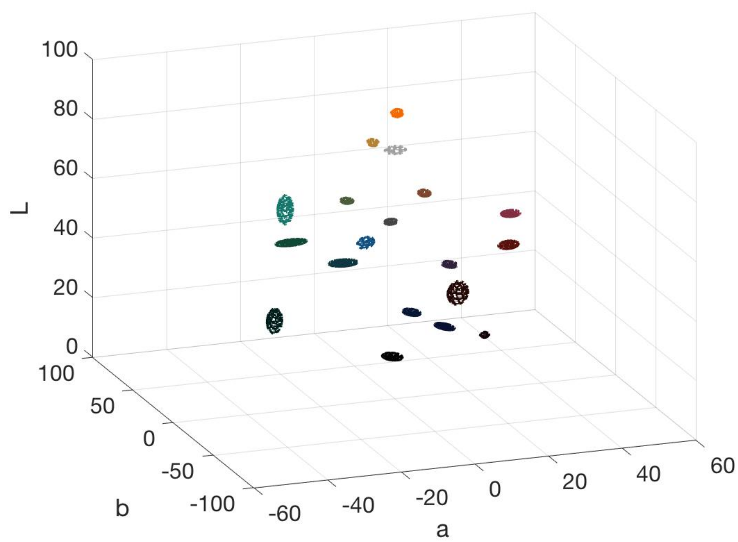

Figure B.15: Estimation of ellipsoids for double bandwidth tuning parameters with the third normalizarion method.

B.6 Estimation results of ellipsoids with combination of the triple bandwidth tuning parameters minimized by the Riemannian metric and three normalization methods

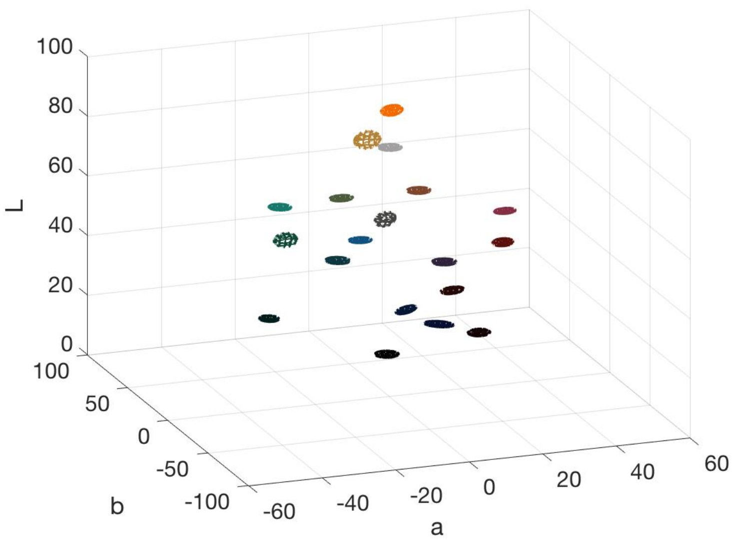

Figure B.16: Estimation of ellipsoids for triple bandwidth tuning parameters with the first normalizarion method.

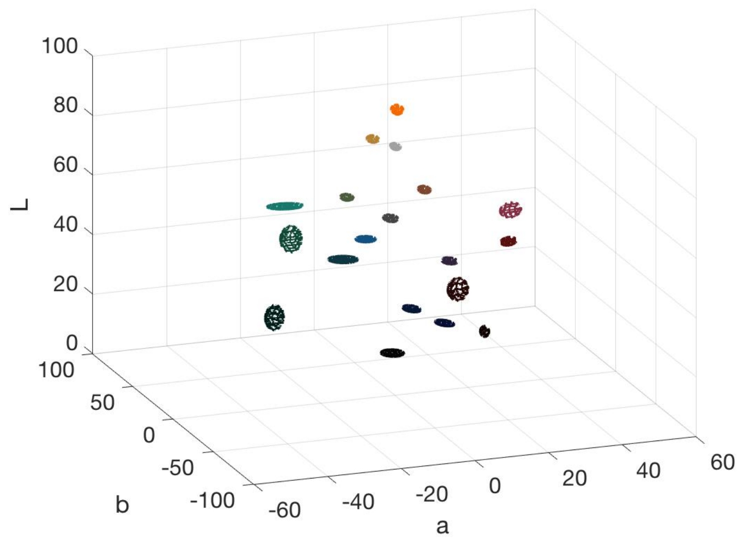

Figure B.17: Estimation of ellipsoids for triple bandwidth tuning parameters with the second normalizarion method.

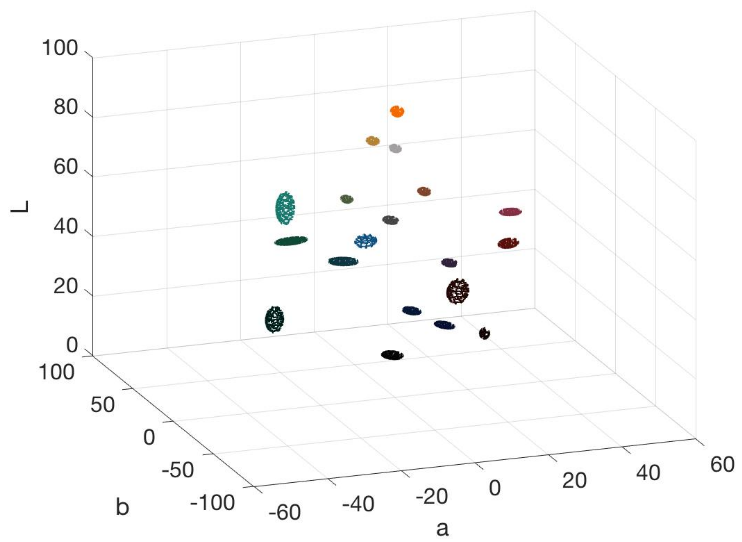

Figure B.18: Estimation of ellipsoids for triple bandwidth tuning parameters with the third normalizarion method.

B.7 Estimation results of ellipsoids with combination of the single bandwidth tuning parameter minimized by the KL divergence and three normalization methods

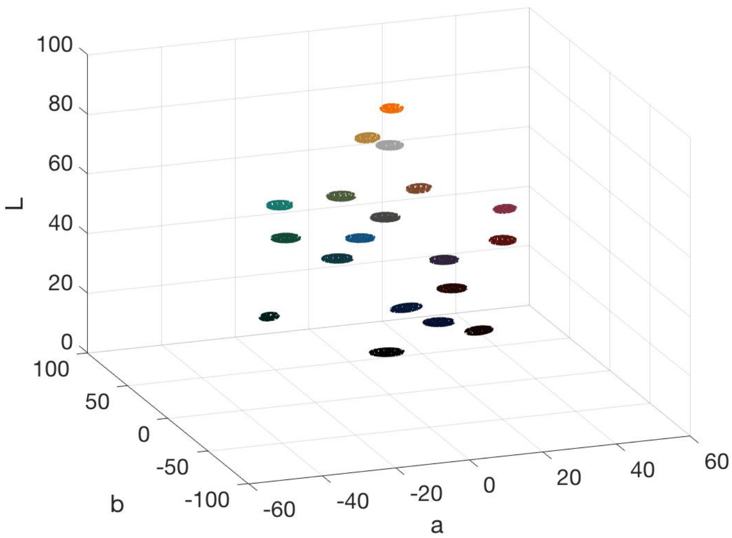

Figure B.19: Estimation of ellipsoids for single bandwidth tuning parameter with the first normalizarion method.

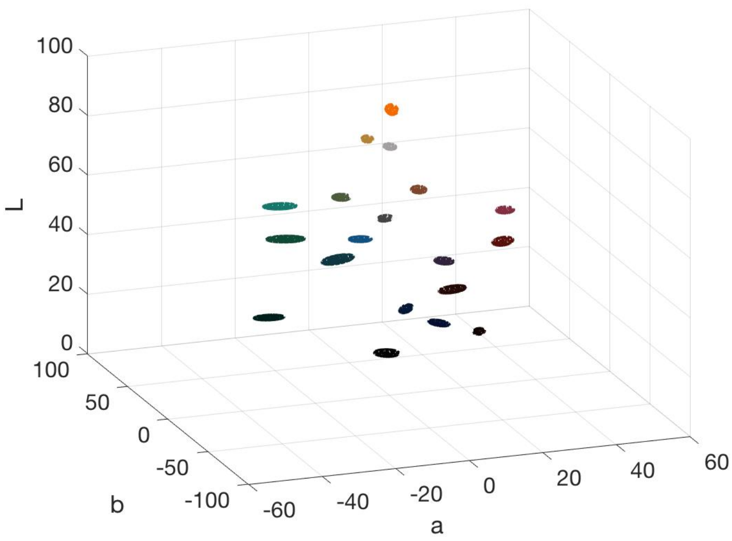

Figure B.20: Estimation of ellipsoids for single bandwidth tuning parameter with the second normalizarion method.

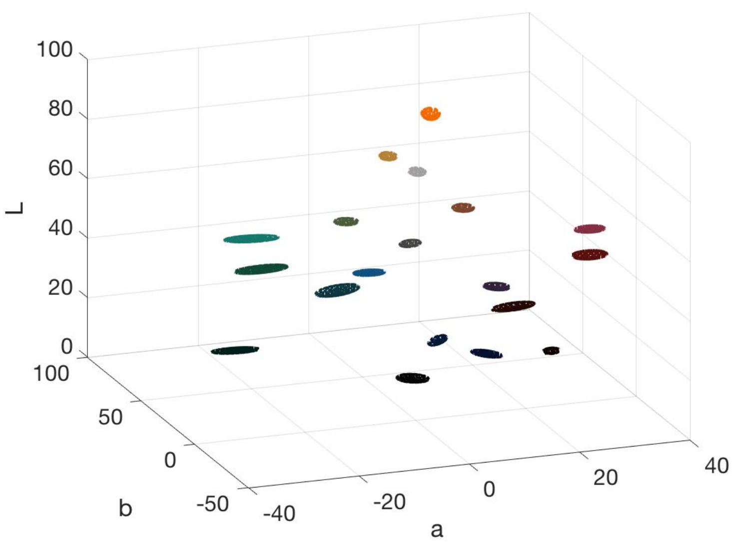

Figure B.21: Estimation of ellipsoids for single bandwidth tuning parameter with the third normalizarion method.

B.8 Estimation results of ellipsoids with combination of the double bandwidth tuning parameters minimized by the KL divergence and three normalization methods

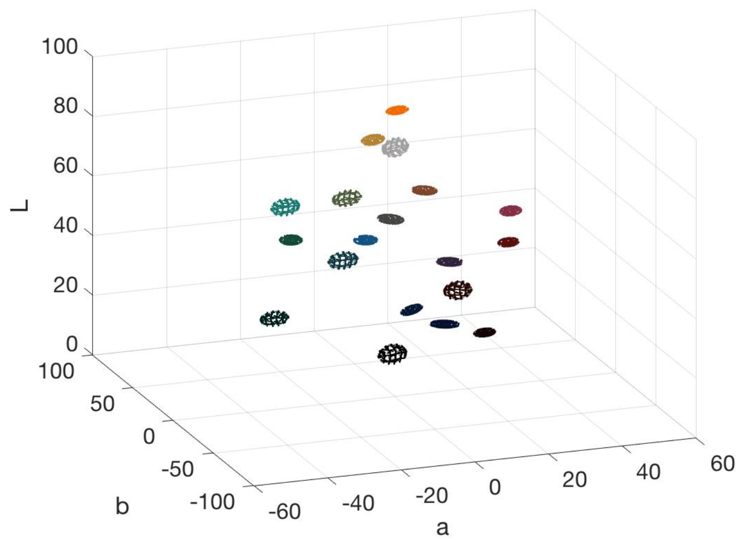

Figure B.22: Estimation of ellipsoids for double bandwidth tuning parameters with the first normalizarion method.

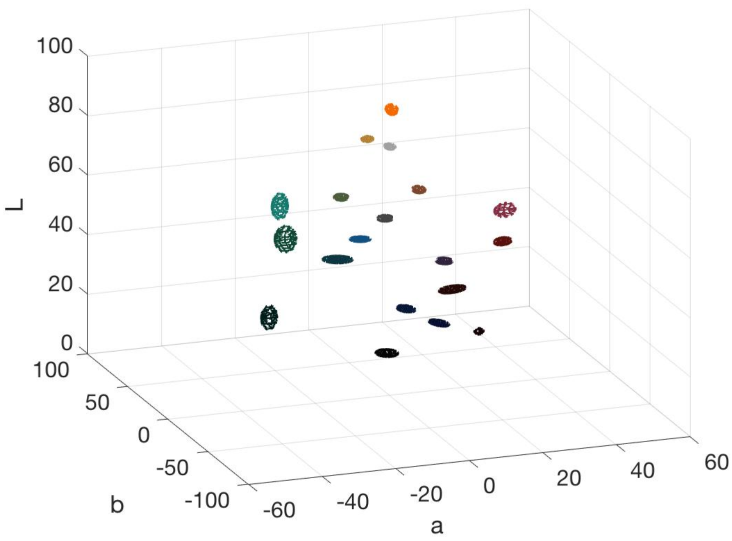

Figure B.23: Estimation of ellipsoids for double bandwidth tuning parameters with the second normalizarion method.

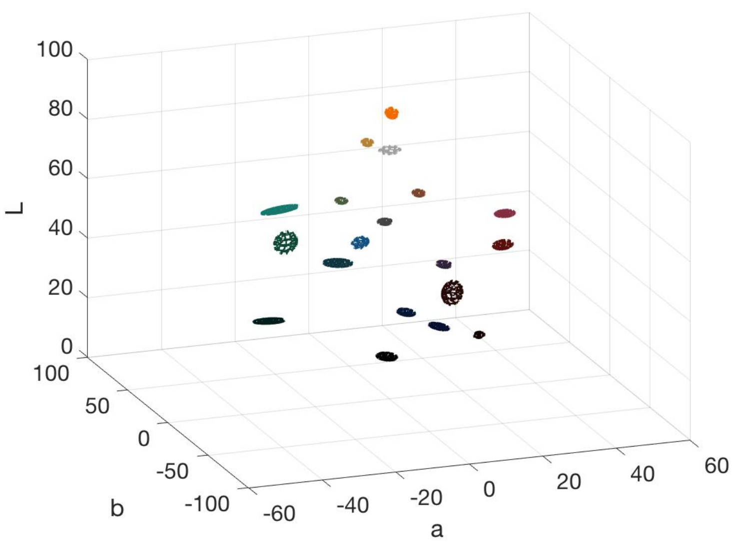

Figure B.24: Estimation of ellipsoids for double bandwidth tuning parameters with the third normalizarion method.

B.9 Estimation results of ellipsoids with combination of the triple bandwidth tuning parameters minimized by the KL divergence and three normalization methods

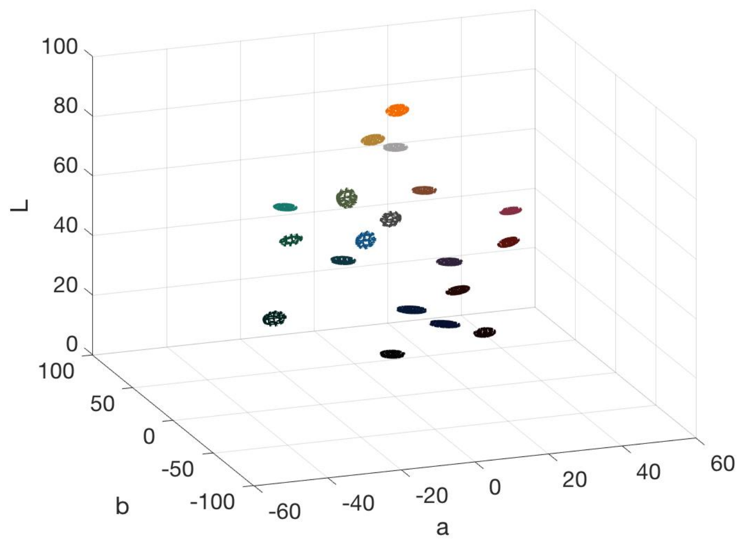

Figure B.25: Estimation of ellipsoids for triple bandwidth tuning parameters with the first normalizarion method.

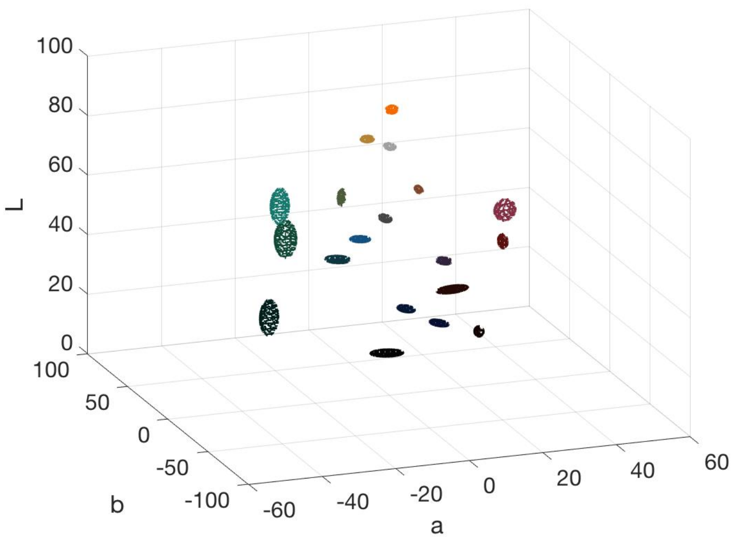

Figure B.26: Estimation of ellipsoids for triple bandwidth tuning parameters with the second normalizarion method.

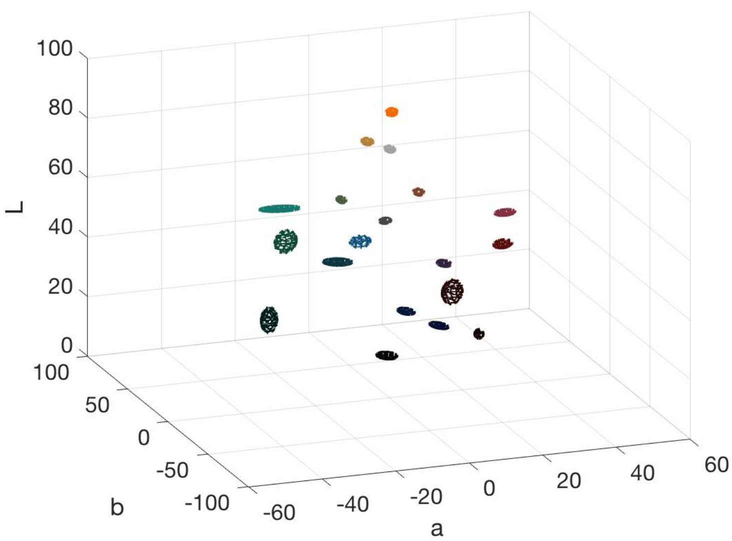

Figure B.27: Estimation of ellipsoids for triple bandwidth tuning parameters with the third normalizarion method.